LABORATORY ASSESSMENT OF TIME-DEPENDENT TENSILE STRENGTH OF MAHA SARAKHAM SALT

Sopon Wisetsaen

A Thesis Submitted in Partial Fulfillment of the Requirements for the

Degree of Master of Engineering in Geotechnology

Suranaree University of Technology

Academic Year 2013

การทดสอบในห้องปฏิบัติการเพื่อหากำลังดึงเชิงเวลาของเกลือหินชุด

มหาสารคาม

นายโสภณ วิเศษแสน

วิทยานิพนธ์นี้เป็นส่วนหนึ่งของการศึกษาตามหลักสูตรปริญญาวิศวกรรมศาสตรมหาบัณฑิต

สาขาวิชาเทคโนโลยีธรณี

มหาวิทยาลัยเทคโนโลยีสุรนารี

ปีการศึกษา 2556

LABORATORY ASSESSMENT OF TIME-DEPENDENT TENSILE STRENGTH OF MAHA SARAKHAM SALT

Suranaree University of Technology has approved this thesis submitted in partial fulfillment of the requirements for a Master's Degree.

Thesis Examining Committee

_____

(Dr. Prachya Tepnarong)

Chairperson

_____

(Assoc. Prof. Dr. Kittitep Fuenkajorn)

Member (Thesis Advisor)

_____

(Dr. Decho Phueakphum)

Member

_____ _____

(Prof. Dr. Sukit Limpijumnong) (Assoc. Prof. Flt. Lt. Dr. Kontorn Chamniprasart)

Vice Rector for Academic Affairs Dean of Institute of Engineering

โสภณ วิเศษแสน : การทดสอบในห้องปฏิบัติการเพื่อหากำลังดึงเชิงเวลาของเกลือหินชุดมหาสารคาม (LABORATORY ASSESSMENT OF TIME-DEPENDENT TENSILE STRENGTH OF MAHA SARAKHAM SALT) อาจารย์ที่ปรึกษา : รองศาสตราจารย์ ดร.กิตติเทพ เฟื่องขจร, 67 หน้า.

การศึกษานี้มีวัตถุประสงค์เพื่อหาค่ากำลังดึงที่ขึ้นกับเวลาของเกลือหิน ด้วยวิธีการทดสอบกำลังดึงแบบวงแหวนภายใต้อัตราการดึงและอุณหภูมิที่ผันแปร ตัวอย่างเกลือหินที่ใช้ในการทดสอบมีขนาดเส้นผ่าศูนย์กลาง 100 มิลลิเมตร นำมาตัดให้มีความหนา 38 มิลลิเมตร และเจาะรูตรงกลางให้มีขนาดเส้นผ่าศูนย์กลาง 31.5 มิลลิเมตร ตัวอย่างเกลือหินถูกกดตามแนวเส้นผ่าศูนย์กลาง ซึ่งสอดคล้องกับอัตราการดึงที่จุดเริ่มแตกที่รูตรงกลางเท่ากับ 3×10^{-5}, 3×10^{-4}, 3×10^{-3}, 3×10^{-2} และ 3×10^{-1} MPa/s การทดสอบผันแปรอุณหภูมิจาก 270 ถึง 375 เคลวิน ผลการทดสอบระบุว่า ค่ากำลังดึงมีค่าเพิ่มขึ้นเมื่ออัตราการดึงที่จุดเริ่มแตกสูงขึ้น และค่ากำลังดึงมีค่าลดลงเมื่ออุณหภูมิสูงขึ้น กฎของเอกซ์โพแนนเชียลสามารถใช้อธิบายพฤติกรรมของเกลือหินที่ขึ้นกับเวลาภายใต้กำลังดึงได้ดี ผลการศึกษาสามารถนำมาคาดคะเนค่ากำลังดึงของเกลือหินที่ขึ้นกับเวลาของหลังคาโพรงเกลือภายใต้การผันแปรอุณหภูมิ เช่น บริเวณรอบโพรงกักเก็บของเสีย

สาขาวิชา เทคโนโลยีธรณี ลายมือชื่อนักศึกษา _____

ปีการศึกษา 2555 ลายมือชื่ออาจารย์ที่ปรึกษา_____

SOPON WISETSAEN : LABORATORY ASSESSMENT OF TIME-DEPENDENT TENSILE STRENGTH OF MAHA SARAKHAM SALT. THESIS ADVISOR : ASSOC. PROF. KITTITEP FUENKAJORN, Ph.D., P.E.

RING TEST/TENSILE STRENGTH/SALT

The objective of this study is to determine the time-dependent tensile strength of rock salt by performing ring tension tests under various loading rates and temperatures. The 100 mm diameter cores are dried-cut to obtain disk shaped specimens with a thickness of 38 mm. The inner diameter is 31.5 mm. A line load is applied along the specimen diameter under various the loading rates which are equivalent to the tensile stress rates induced at the crack initiation point of 3×10^{-5}, 3×10^{-4}, 3×10^{-3}, 3×10^{-2} and 3×10^{-1} MPa/s. The testing temperatures are varied from 270 to 375 Kelvin. The results indicate that the tensile strength increases with the loading rate, and decreases with increasing temperatures. The exponential law can well describe the time-dependent behavior of salt under tension. The findings can be used to estimate the time-dependent tensile strength of salt roof under various isothermal conditions, such as those around waste storage openings.

School of Geotechnology Student's Signature

Academic Year 2012 Advisor's Signature

ACKNOWLEDGMENTS

I wish to acknowledge the funding supported by Suranaree University of Technology (SUT).

I would like to express my sincere thanks to Assoc. Prof. Dr. Kittitep Fuenkajorn for his valuable guidance and efficient supervision. I appreciate his strong support, encouragement, suggestions and comments during the research period. My heartiness thanks to Dr. Prachya Tepnarong and Dr. Decho Phueakphum for their constructive advice, valuable suggestions and comments on my research works as thesis committee members. Grateful thanks are given to all staffs of Geomechanics Research Unit, Institute of Engineering who supported my work.

Finally, I would like to thank beloved parents for their love, support and encouragement.

Sopon Wisetsaen

TABLE OF CONTENTS

Page

TABLE OF CONTENTS (Continued)

Page

LIST OF TABLES

Table **Page**

LIST OF FIGURES

LIST OF FIGURES (Continued)

Figure **Page**

LIST OF FIGURES (Continued)

Figure **Page**

LIST OF SYMBOLS AND ABBREVIATIONS

A	=	Fourier coefficients
B	=	Fourier coefficients
D	=	Disk diameter
E	=	Tensile elastic modulus for equation 6.2 and 6.7
P	=	Applied load
T	=	Absolute temperature
t	=	Disk thickness related to σ_{Ring}
t	=	Time
χ	=	Empirical constant related to $\sigma_{R,F}$ and $\partial\sigma_{\theta}/\partial t$
ι	=	Empirical constant related to $\sigma_{R,F}$ and $\partial\sigma_{\theta}/\partial t$
ν	=	Poisson's ratio
α	=	Stress constant
β	=	Stress exponent
κ	=	Time exponent
λ	=	Temperature constant
ψ	=	Empirical constant related to E and T
A'	=	Empirical constant related to $\sigma_{R,F}$ and t (time)
B'	=	Empirical constant for equation $\sigma_{R,F}$ and t (time)
$\bar{r}$	=	Relative hole radius
r_i	=	Hole radius

LIST OF SYMBOLS AND ABBREVIATIONS (Continued)

r_o	=	Disk radius
E_0	=	Tensile elastic modulus at 0 Kelvin related to E and T
k_F	=	Stress concentration factor
K_F	=	Stress concentration factor at the hole boundary
P_f	=	Maximum of loading at failure load
ε_t	=	Total tensile strain
ε_e	=	Instantaneous strain
ε_p	=	Permanent strain
ε_t^e	=	Elastic tensile strain
ε_t^c	=	Transient creep
σ_1	=	Maximum principal stress
σ_2	=	Minimum principal stress
σ_3	=	Confining pressures
σ_B	=	Brazilian tensile strength
σ_C	=	Uniaxial compressive strengths
σ_m	=	Mean stress
σ_R	=	Constant stress rate
σ_r	=	Radial stress
$\sigma_{R,F}$	=	The salt Tensile strength

LIST OF SYMBOLS AND ABBREVIATIONS (Continued)

σ_{Ring}	=	Ring test tensile strength
σ_t	=	Tensile stress
σ_θ	=	Tangential stress
$\partial\sigma_1/\partial t$	=	Loading rates
$\partial\sigma_\theta/\partial t$	=	Stress rates at the crack initiation point
τ_{oct}	=	Octahedral shear stress
γ_{oct}	=	Octahedral shear strain

CHAPTER I

INTRODUCTION

1.1 Background and rationale

Tensile strength and deformability of rock salt is an important parameter used in the design and stability analysis of underground structures. The rock tensile strength dictates the maximum roof span of underground openings, the maximum internal pressure of unlined storage caverns and the borehole pressure for hydraulic fracturing (Fuenkajorn and Klanphumeesri, 2010). The effect of temperatures on rock salt has been largely concentrated on the time-dependent creep deformation under compression (Carter and Hansen, 1983; Liang et al., 2006; Fuenkajorn et al., 2012). Study on the time-dependent effect on the salt tensile strength under low and elevated temperatures has been very rare.

1.2 Research objectives

The objective of this study is to determine the time-dependent tensile strength of the Maha Sarakham salt under temperatures ranging from 270 to 375 Kelvin (0–100 Celsius). Ring tension test are performed to measure the tensile creep strains and failure of the salt specimen at the crack initiation point. The finite difference method is performed to confirm of the stress distribution of the ring test specimen under the diametral loading and the distribution of the normalized tangential and radial stresses along loading diameter. The applied loading rates are varied which are equivalent to the tensile stress rates at the crack initiation point from 0.00003,

0.0003, 0.003, 0.03 to 0.3 MPa/s. The specimen deformations are monitored with two strain gages to calculate the tensile strains. The test results are used to calibrate the deformability and strength of the salt rock specimens, creep parameters and stress-strain with time dependency under various constant temperatures. A time-dependent tensile strength criterion is developed.

1.3 Research methodology

The research methodology shown in Figure 1.1 comprises 8 steps; including literature review, sample preparation, computer simulation, laboratory testing, calibration of tensile creep equation, discussions and conclusions and thesis writing.

1.3.1 Literature review

Literature review is carried out to study the previous researches on time-dependent behavior of rock salt as affected by mechanical and thermal loadings. The sources of information are from text books, journals, technical reports and conference papers. A summary of the literature review is given in chapter two.

1.3.2 Sample preparation

The salt specimens are prepared from 100 mm salt cores drilled from the depths ranging between 70 m and 120 m by Asean Potash Mining Co. in the northeast of Thailand. The salt cores belong to the Middle Salt member of the Maha Sarakham formation. Sample preparation is carried out in the laboratory at Suranaree University of Technology. Samples are prepared for ring tension test. The specimens are drilled and dried-cut to obtain disk specimens with a thickness of 38 mm with a center hole diameter of 31.5 mm. Strain gages are installed to measure

tensile strain at the inner hole wall where the tensile crack is initiated. After preparation the specimens are wrapped with plastic sheet at all time to prevent it from subjecting to the surrounding humidity. No bedding is observed in the specimens. Over 20 specimens are used for this study.

1.3.3 Computer simulations

The finite difference analysis is performed to compare the stress distribution in the ring test specimen under the diametral loading with the close-form solution. The distribution of the normalized tangential stress (σ_θ/P) and radial stress (σ_r/P) along loading diameter will be determined from finite difference analysis. The model dimensions are identical is used in the test.

1.3.4 Laboratory testing

The ring tension test is applied loading rates are varied which are equivalent to the tensile stress rates at the crack initiation point from 0.00003, 0.0003, 0.003, 0.03 to 0.3 MPa/s. The electronic load cell is used to record loading increasing. The load at failure is recorded to calculate the salt tensile strength. The specimen deformations are monitored with two strain gages to calculate the tensile strains. Photographs are taken of the failed specimens.

1.3.5 Tensile creep equation

The results are used to determine the elastic and transient creep parameters. The regression analysis of the tensile creep strain equation with the IBM SPSS Statistics 19 (SPSS) is performed to determine the elastic and creep parameters.

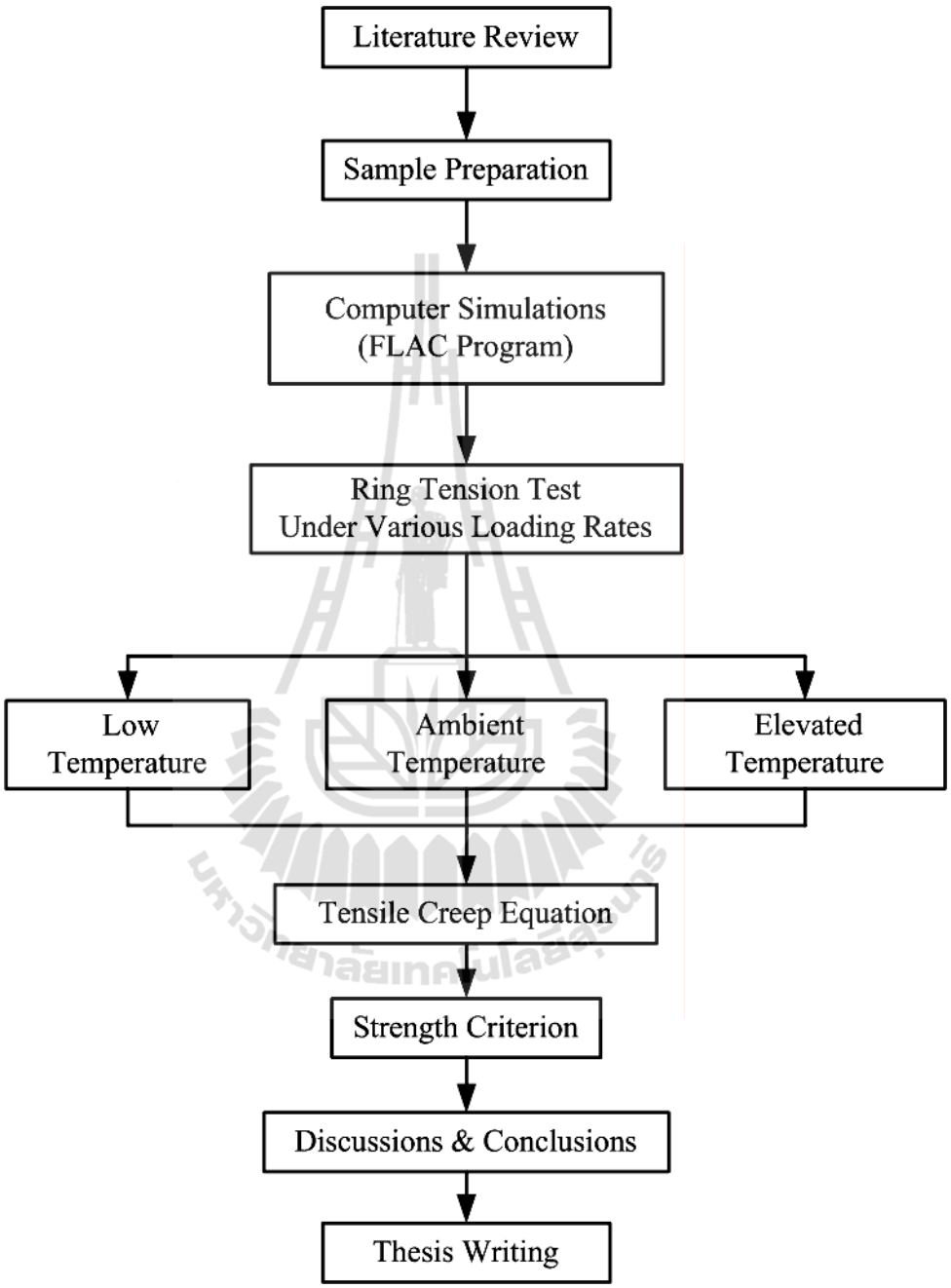

Figure 1.1 Research methodology.

1.3.6 Strength criterion

Results from laboratory measurements in terms of the tensile strength of rock salt are used to formulate mathematical relations. The objective is to predict the tensile strength under low and elevated temperatures as a function of time.

1.3.7 Conclusion and thesis writing

All research activities, methods, and results will be documented and complied in the thesis. The research or findings will be published in the conference proceedings or journals.

1.4 Scope and limitations

The scope and limitations of the research include as follows.

1. All tests are conducted on rock salt specimens obtained from the Middle Salt member of the Maha Sarakham formation in northeastern Thailand.
2. The applied loading rates vary from 0.00003, 0.0003, 0.003, 0.03 to 0.3 MPa/s at the crack initiation point.
3. The testing temperatures range from 270 to 375 Kelvin.
4. Testing is made under dry condition.
5. Up to 20 samples are tested.
6. The disk specimens are 100 mm diameter with 31.5 mm center hole and 38 mm thickness.
7. Numerical simulations using FLAC is performed to determine the stress distribution of the ring test specimen under the diametral loading.

8. The research findings are published in conference paper or journal.

1.5 Thesis contents

This first chapter introduces the thesis by briefly describing the rationale and background and identifying the research objectives. The third section identifies the research methodology. The fourth section describes scope and limitations. The fifth section gives a chapter by chapter overview of the contents of this thesis.

The second chapter summarizes results of the literature review. Chapter three describes samples preparation. The computer simulations are describes in chapter four. The laboratory tests and results of all tested are presented in chapter five. The tensile creep model and strength criterions are describes in chapter six. Chapter seven provides the conclusion and recommendations for future research studies.

CHAPTER II

LITERATURE REVIEW

2.1 Introduction

The topics reviewed here include mechanical properties of rock salt, factor influencing mechanical properties of rock salt, factor influencing deformation of rock, and ring tension tests.

2.2 Mechanical Properties of Rock Salt

Rock salt has very complicated engineering behavior. Its behavior is affected by many factors, such as crystal size, bonding between crystal, time, temperature, inclusions and humidity etc. Deformation and creep properties exhibit the effect on rock salt characteristics by these factors (Fuenkajorn et al., 2012; Yanan et al., 2010; Kensakoo et al., 2007; Fuenkajorn and Daemen, 1988; Varo and Passaris, 1977)

The time-dependent deformation (or creep) is the process at which the rock can continue deformation without changing stress. The creep strain seldom can be recovery fully when loads are removed, thus it is largely plastic deformation. Creep deformation occurs in three different phases, as shown in Figure 2.1, which relatively represents a model of salt properties undergoing creep deformation due to the sustained constant load (Jeremic, 1994). Upon application of a constant force on the rock salt, an instantaneous elastic strain (ε_e) is induced. The elastic strain is followed by a primary or transient strain, shown as Region I. Region II, characterized by an almost constant slope in the diagram, corresponds to secondary or steady state creep.

Tertiary or accelerating creep leading to rather sudden failure is shown in Region III. Laboratory investigations show that removal of applied load in Region I at point L will cause the strain to fall rapidly to the M level and then asymptotically back to zero at N. The distance LM is equal to the instantaneous strain ε_e. No permanent strain is induced here. If the removal of stress takes place in the steady-state phase the permanent strain (ε_p) will occur. From the stability point of view, salt structure deformations after constant load removal have only academic significance, since the stresses imposed underground due to mining operations are irreversible.

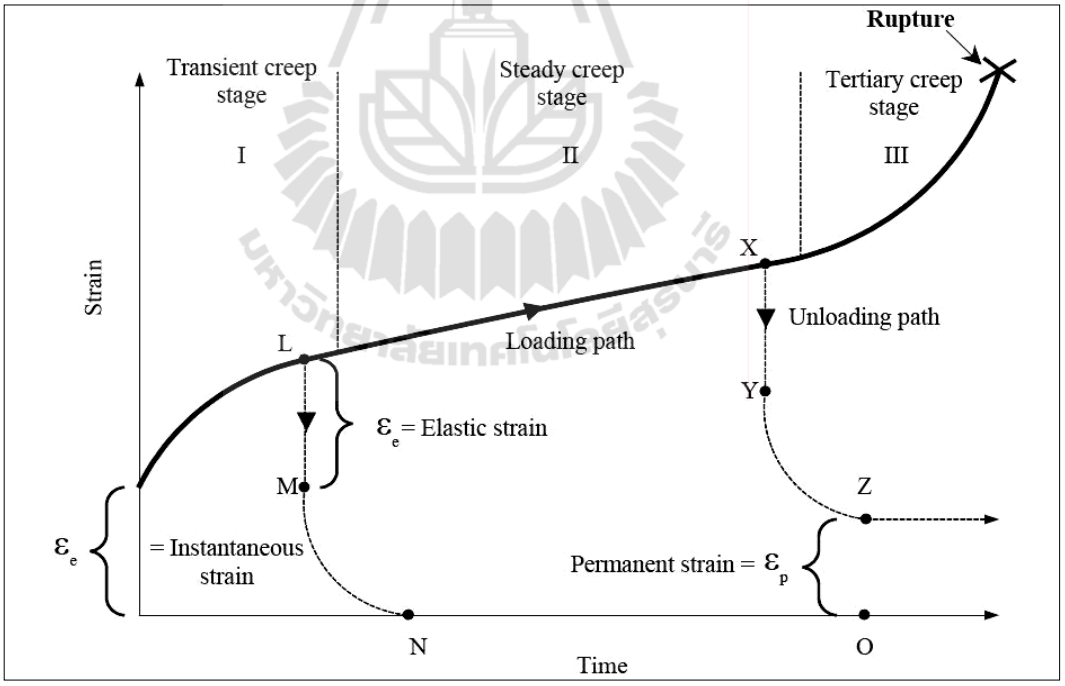

Figure 2.1 The typical deformation as a function of time of creep materials (modified from Jeremic, 1994).

The behavior of the salts with time-dependent deformation under constant load is characterized as a visco-elastic and visco-plastic phenomenon. Under these

conditions the strain criteria are superior to the strength criteria for design purposes, because failure of most salt pillars occurs during accelerated or tertiary phase of creep, due to the almost constant applied load.

A typical stress versus strain curve for a rock specimen under static loading can be divided into four regions as revealed in Figure 2.2. In region I there is a small foot in the curve, and the observed modulus is lower because of the nonelastic strain arising from the closing up of the microcracks and pore. Region II represents the true modulus of the bulk material and the stress versus strain curve here is linear. The stress-strain curve then starts to deviate from linearity in region III indicating the stage of nucleation of microcracks. Here there is a general loosening of the grain boundaries which is not yet obvious in microscopic observations. Only in region IV do microcracks become visible in an optical microscope. The only difference was that regions III and IV of the static stress-strain curve were extended to larger strains. Consequently the fracture strength was increased primarily because of a larger strain-to-fracture (Kumar, 1968; Liang et al., 2010).

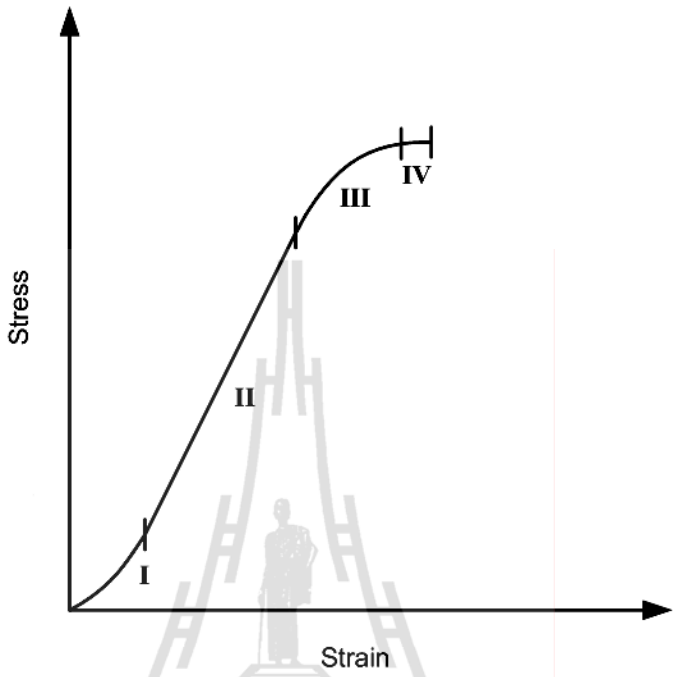

Figure 2.2 A typical stress-strain curve for rock materials (Kumar, 1968; Liang et al., 2010).

The total tensile strain at the crack initiation point in salt ring is divided in two parts, elastic strain (linear and recoverable strain) and plastic creep strain (time-dependent and nonrecoverable strain):

$$\varepsilon_t = \varepsilon_t^e + \varepsilon_t^c \tag{2.1}$$

where ε_t is the total tensile strain, ε_t^e is elastic tensile strain, ε_t^c is transient creep tensile strains. The elastic strain is calculated from the current stress state using classical elastic theory (Jaeger et al., 2007).

$$\varepsilon_t^e = \frac{\sigma_t}{E} \tag{2.2}$$

where σ_t is the tensile stress, ε_t^e is the elastic tensile strain, E is the tensile elastic modulus.

Exponential law is applied to describe the time-dependent behavior of salt. The law in derived by linking the creep strain to stress and temperature. The exponential law presents the transient creep strain as a function of stress, time and temperature in exponential form (Senseny, 1983).

$$\varepsilon_t^c = \alpha \cdot \sigma_t^\beta \cdot t^\kappa \cdot \exp(-\lambda/T) \tag{2.3}$$

where α is stress constant, β is the stress exponent, κ is time exponent, λ is temperature constant, and T is the absolute temperature.

2.3 Factors Influencing Mechanical Properties of Rock Salt

Senseny (1984) studies the influence on creep of specimen size of salt for transient and steady –state deformation. Two specimen sizes, 10 mm and 50 mm diameter cylinders with a length to diameter ration of 3.0, were investigated by means of triaxial compression creep testing under various temperatures. The results were fitted to potential creep laws that steady –state creep does not. The rate of transient creep strain of the small specimens is higher than that of larger specimens. This implies that constitutive laws developed from laboratory data may over predict deformation measured in the field, especially if the formulation results largely from transient creep.

Fokker (1998) studies that effect of grain size on the creep behavior and strength of the rock salt and field condition. The average grain size of the salt visually observed from the core and post failure specimens were 5mm x 10mm x

10mm. It was concluded that the large size of the salt crystals increases the effect of the crystallographic features on the mechanics of deformation and failure of the samples.

Study by Franssen and Spiers (1990), Raj and Pharr (1992) and Senseny et al. (1992) concludes that the shear strength and deformation of halite crystals are orientation dependent. The small size of the sample may not provide good representative test results. This also reflects on the specifications by ASTM (ASTM D2664, D2938 and D3967). The ASTM standard methods specify that to minimize the effect of grain size the sample diameter should be at least ten times the average grain size.

Inclusions and impurities in salt have an effect on to the creep deformation and strength of salt. The degree of impurity is varying for different scales of the rock salt. On a small scale, such as for laboratory specimens, the impurities of salt involve ferruginous inclusions and thin clay seams along grain boundaries or bedding planes. The impurities distribute uniformly in the salt may affect the strength of rock salt. This can decrease the creep deformation and strength of rock salt. These phenomena have been reported by Franssen and Spiers (1990), Raj and Pharr (1992) and Senseny et al. (1992), as well.

Bonding between grains can affect the creep rate and the strength of salt. The bonding between the crystals is weak in rock salt. Allemandou and Dusseault (1996) observe the post –failure from the Brazilian strength test and uniaxial compressive strength tests. They report that stress depends on the boundary between grains and crystals.

2.4 Factor Influencing Deformation of Rock

2.4.1 Loading Rate

Sangha and Dhir (1972) studied of the influence of strain rate on the strength, deformation and fracture properties of Lower Devonian sandstone are presented. Strain rates were varied between 2.5×10^{-3}/sec to 2.5×10^{-9}/sec. A new criterion, based on the incremental Poisson's ratio, capable of predicting both the long-term strength of a material and also able to establish whether a material under load is safe from long-term failure is suggested. This criterion is based on short-term creep tests and substantiated by the constant strain-rate strength results. Comparison of strength results obtained at different rates of loading and rates of straining showed that for similar loading times to failure the constant rates of loading gave slightly higher strength values. Modes of rupture were found to be independent of both loading methods but dependent upon time taken to reach strength failure.

Ma and Daemen (2006) study the strain rate dependent strength and stress-strain characteristics of a welded tuff. Results of 61 uniaxial compression tests on the welded Topopah Spring tuff are presented. The tests were carried out under constant strain rates at room temperature. Stress–strain analysis indicates that dilatancy and compaction start at about 50% of ultimate strength. A sudden stress drop occurs at about 90% of the ultimate strength, which indicates the onset of specimen failure. Both strength and peak axial strain decrease with strain rate as power functions. Based on the strain rate dependence of strength and peak axial strain, it is inferred that the elastic modulus is strain rate dependent. A relationship between stress, axial strain, and axial strain rate is developed. The parameters in this

relation are estimated using multivariate regression to fit stress–axial strain–strain rate data.

Kenkhunthod and Fuenkajorn (2010) study the influence of loading rate on deformability and compressive strength of three Thai sandstones. Uniaxial and triaxial compressive strength tests have been performed using a polyaxial load frame to assess the influence of loading rate on the strength and deformability of three Thai sandstones. The applied axial stresses are controlled at constant rates of 0.001, 0.01, 0.1, 1.0 and 10 MPa/s. The confining pressures are maintained constant at 0, 3, 7 and 12 MPa, as shown in Figure 2.3. The sandstone strengths and elastic moduli tend to increase exponentially with the loading rates. The effects seem to be independent of the confining pressures. An empirical loading rate dependent formulation of both deformability and shear strength is developed for the elastic and isotropic rocks. It is based on the assumption of constant distortional strain energy of the rock at failure under a given mean normal stress. The proposed multiaxial criterion well describes the sandstone strengths within the range of the loading rates used here. It seems reasonable that the derived loading rate dependent equations for deformability and shear strength are transferable to similar brittle isotropic intact rocks.

Fuenkajorn et al. (2012) studied the effects of loading rate on strength and deformability of the Maha Sarakham salt. The uniaxial and triaxial compression tests have been performed to assess the influence of loading rate on the compressive strength and deformability of the Maha Sarakham salt. The lateral confining pressures are maintained constant at 0, 3, 7, 12, 20 and 28 MPa while the axial stresses are increased at constant rates of 0.001, 0.01, 0.1, 1.0 and 10 MPa/s until failure occurs. It was also found that the salt elasticity and strength increase with the

loading rates, as shown in Figure 2.4. The elastic (tangent) modulus determined at about 40% of the failure stress varies from 15 to 25 GPa, and the Poisson's ratio from 0.23 to 0.43. The elastic parameters tend to be independent of the confining pressures. The strains induced at failure decrease as the loading rate increases.

Liang et al. (2010) state that effect of strain rate on the mechanical properties of salt rock. For the experiment, three uniaxial compression displacement rates were chosen, leading to $\dot{\varepsilon}$ values of 2.0×10^{-5}, 2.0×10^{-4} and 2.0×10^{-3}/s, a factor of 100. Each of the six rock salt specimens was assigned to be tested under one loading strain rate, and the two thenardite specimens was tested under the two lower strain rates of $2.0\times10^{-5}$and 2.0×10^{-4}/s. The strength of salt rock is only slightly affected by loading strain rate. The elastic modulus slightly increases with strain rate, but the increment is small. Under the same strain rate, the strength of thenardite is somewhat larger than rock salt, mainly related to crystal grain size and fabric of the minerals. With strain rate increase, Poisson's ratio of salt rock decreases somewhat and the lateral deformation capacity is diminished. The strain rate also affects the strain of salt rock before it yields (peak strength). The strain at the point of peak strength decreases with strain rate increase. A logarithmic relationship between deformation modulus and loading strain rate was observed in our case: $E_0=0.2\cdot\ln\cdot\dot{\varepsilon}+3.2$. The failure style of salt rock does not change with strain rate variation, and this is different from brittle rock. The failure of halite is mainly in the style of brittle fracture with a bit of shear failure where as that of thenardite is in the style of shearing along a planar surface. The strong viscous deformation ability of salt rock makes it able to absorb energy during uniaxial compression. The resulting internal lateral compression effect

in the specimen is diminished, so the strength and failure style of salt rock almost do not change with loading strain rate.

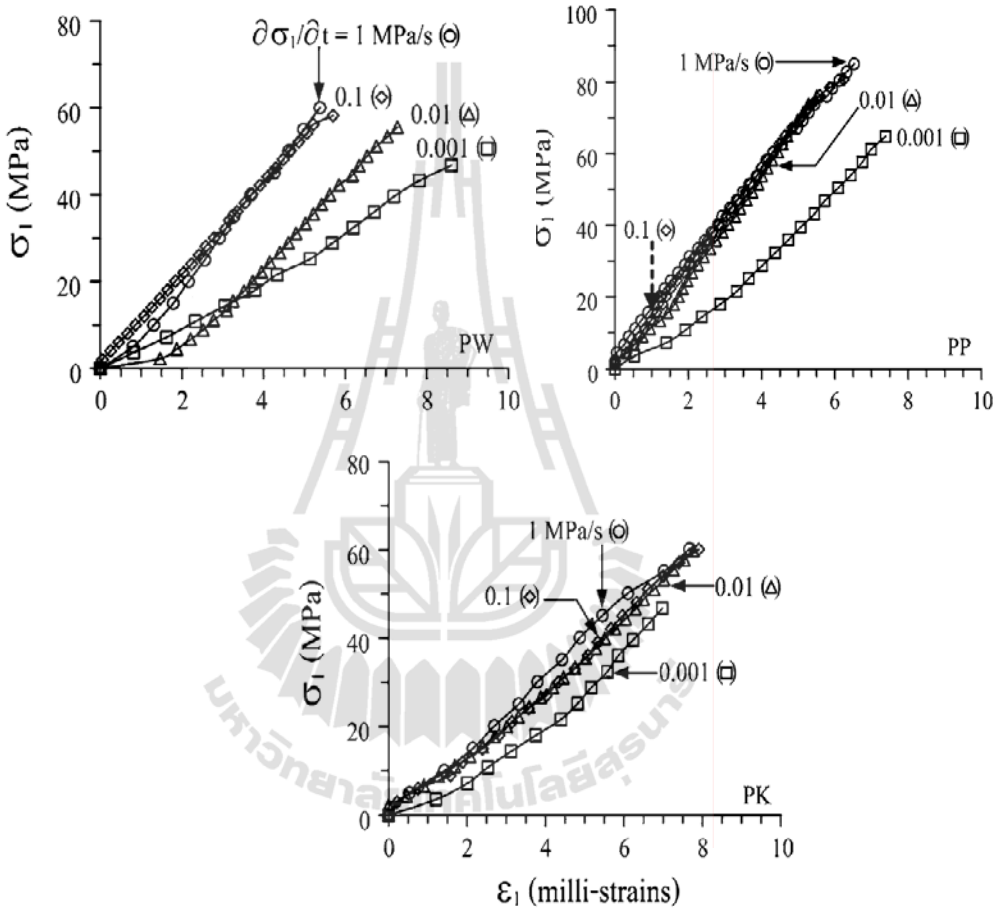

Figure 2.3 Uniaxial compressive strengths under loading rates varied from 0.001, 0.01, 0.1 and 1.0 MPa/s, for PW, PP and PK sandstones (Kenkhunthod and Fuenkajorn, 2010).

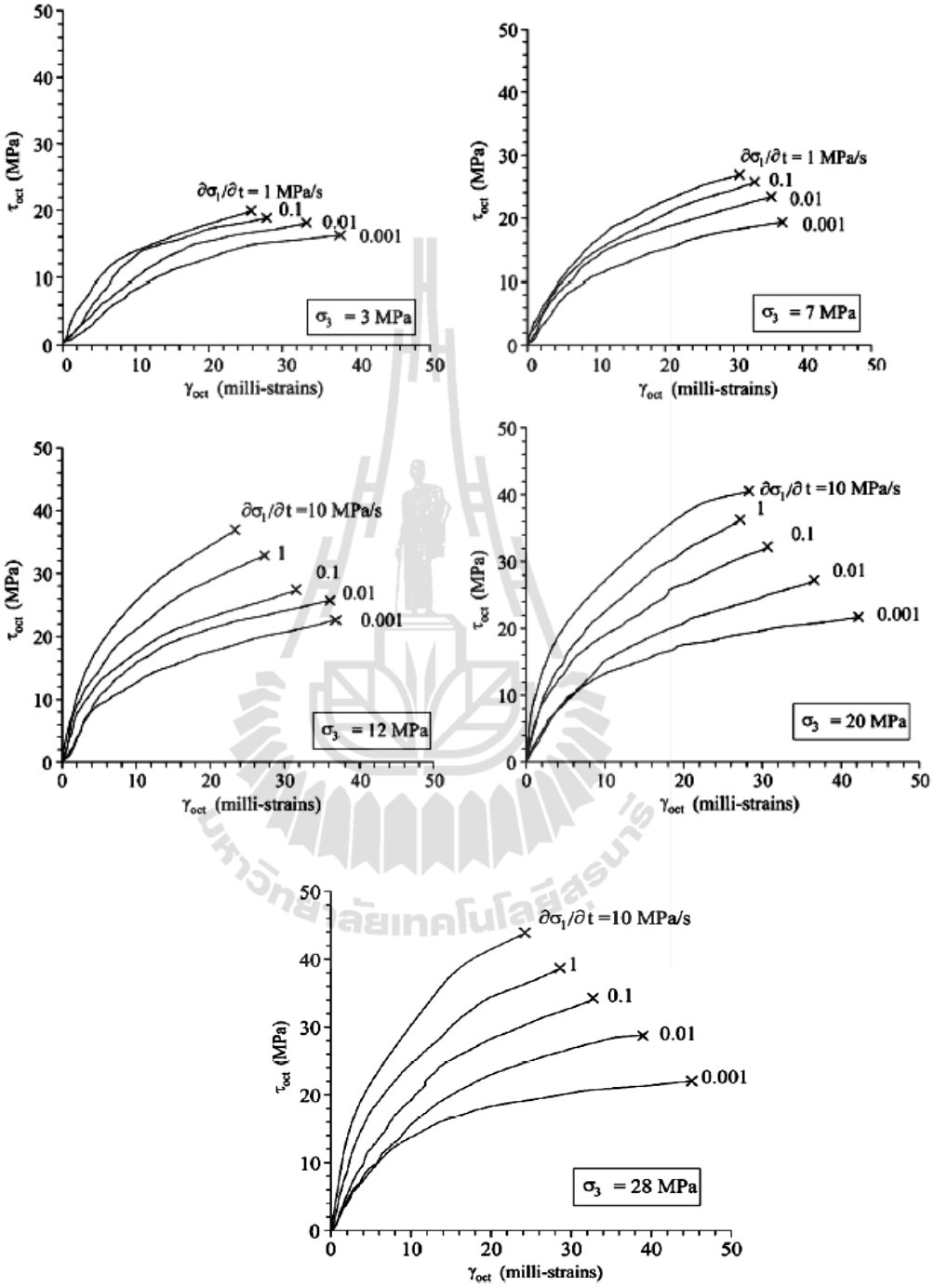

Figure 2.4 Octahedral shear stress (τ_{oct}) as a function of octahedral shear strain (γ_{oct}) for various confining pressures (σ_3) and loading rates ($\partial\sigma_1/\partial t$) (Fuenkajorn et al., 2012).

Ray et al. (1999) describe the effect of cyclic loading and strain rate on the mechanical behaviour of sandstone. The results indicate that the percentage decrease in uniaxial compressive strength was found to increase with the increase in applied stress level and direct proportionality between the two parameters was found. The uniaxial compressive strength of Chunar sandstone was determined at strain rates of 2.5×10^{1}/s, 2.5×10^{0} and 2.5×10^{-1}/s and found to be 99.5 MPa, 75.1 MPa and 64.0 MPa, respectively (Figure 2.5). A clear increase in uniaxial compressive strength was, therefore, observed with increase in strain rate. The failure strength was found to increase with the increase of strain rate and an abrupt increase in strength was noticed at the strain rate of 2.5×10^{1}/s. Fatigue stress was found to increase with the increase in strain rate and Young's modulus was found to increase with the increase in strain rate (Figure 2.6).

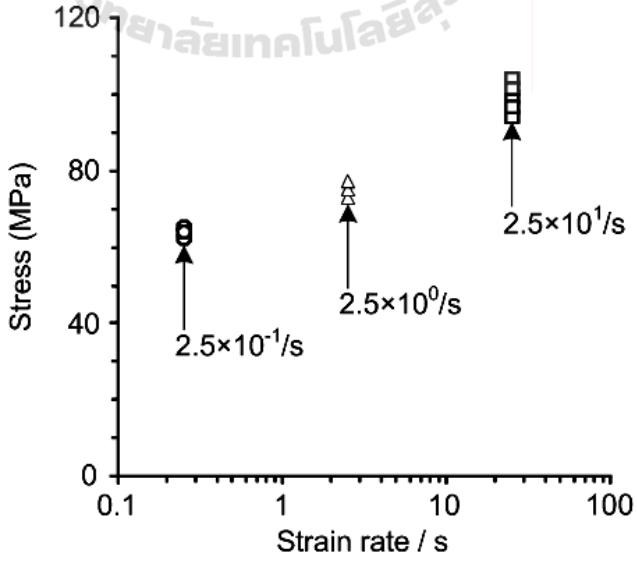

Figure 2.5 Stress as function of strain rate (Ray et al., 1998).

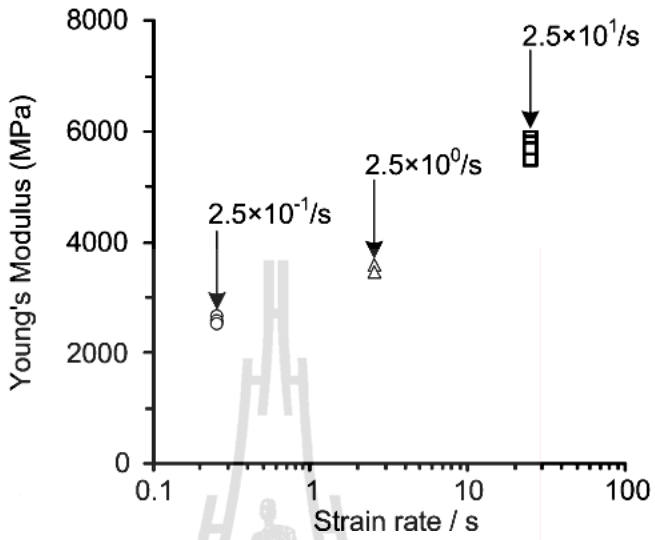

Figure 2.6 Young's modulus as function of strain rate (Ray et al., 1998).

2.4.2 Temperature

Kumar (1968) states that the effect of stress rate and temperature on the strength of basalt and granite. The ultimate strengths of basalt and granite were measured over a range of stress rates from 2×10 to 3×10^{10} psi per second. A comparison of basalt and granite showed that, although their static strength was close, their dynamic strengths were different. The static strengths of basalt and granite were 27.5 and 29 kpsi respectively at the stress rate of 2×10 psi per second while their strengths at the stress rate of 3×10^{10} psi per second were 59 and 70 kpsi respectively. In order to obtain an insight into the basic mechanisms of rock fracturing, the combined effects of stress rate and temperature were studied. The strength of basalt was increased from 27.5 kpsi at room temperature to 45 kpsi at liquid nitrogen temperature at the stress rate of 2×10 psi per second. The mechanisms of fracturing were thermally activated. The activation energy for basalt at 50 kpsi equaled 450 calories per mole.

Considerable information on the experimental work on salt under temperature ranging between 20°C and 200°C and at confining pressure of 200 MPa was documented by Arieli et al. (1982). The intracrystalline flow in synthetic salt is essentially controlled by dislocation glide, at differential stresses above 10-20 MPa. At lower stresses and higher temperatures, the flow is generally controlled by dislocation climb processes.

Charpentier (1984) proposes the time-dependent behavior of rock salt under temperature has guided the "Laboratorie de Mecanique des Solides" to develop specific creep equipment. The design and capacity of this creep test installation offer the possibility of studying a wide range of materials. Considering the characteristics of the problem the "Laboratorie de Mecanique des Solides" has designed a specific creep equipment to carry out long term at high temperature. At present, the experimental installation of three temperature levels between 20°C and 200°C for uniaxial creep. The specimens used are cylinders of 7 cm in diameter and 16 cm in height on Bresse salt. Two specimens test at 20°C applies the uniaxial stresses of 15.3 MPa and 17.8 MPa correspond respectively to 65% and 75% of the uniaxial compressive strength. The creep was observed during two months. At this stage the strain rate is not stable yet and they are still in a transient phase for the two samples. This primary creep can be interpreted by means of a time – hardening law. Test at 100°C applies the uniaxial stresses of 11.3 MPa and 15.3 MPa correspond respectively to 65% and 75% of the uniaxial compressive strength. During about 30 days the values of $\dot{\varepsilon}$ are 13×10^{-6} hr^{-1} and 18×10^{-6} hr^{-1}. For the most severely loaded sample, the increase of the strain rate after two months denotes the existence of a

tertiary state which can probably lead to failure. Three specimens obtained on test at 200°C. The uniaxial stresses of 3.4 MPa, 5 MPa and 7.5 MPa correspond respectively to 20%, 30% and 45% of the uniaxial compressive strength. For the two specimens with the highest levels of load the creep is very important, the strains are 15% and 25% after about two months. This fact shows the major effect of temperature on the time-dependent behavior of rock salt. For the specimens with the smallest load, they have measured only 2% of strain after two months. This difference leads us to consider a yielding point for the behavior law of our rock salt.

Hansen (1984) study the physical and mechanical variability of natural rock salt for four experimentally deformed rock salt in the United States. The influence on creep deformation of impurity content decreases as temperature increases. The rate controlling deformation mechanism shows similar stress and temperature dependency for each salt, being independent of purity. Dislocation glide dominates the deformation at low temperature, i.e. 25°C; whereas at high temperature, i.e. 200°C dislocation climb is the predominant mechanism.

Temperature or heating affects the creep deformation, because they increase the plastic property of salt and long-term deformation (Pudewills et al., 1995). Jeremic (1994) postulates that rock salts lose their brittleness after extension tempering at approximately 600 °C and exhibit a critical shear stress up to 1 MPa. Hamami et al. (1996) study the effect of temperature and conclude that the temperature increase, as for the deviatoric stress, results in an increase of the material deformation. Cristescu and Hunsche (1996) study the temperature effect on the strain rate suitable for laboratory testing. They suggest that the appropriate strain rate for testing at 100 °C and 200 °C is 10^{-8} s^{-1} and 10^{-7} s^{-1} because the temperature

can affect the creep deformation and strength of salt under high temperatures.

Sriapai et al. (2012) study of the temperature effects on salt strength by incorporating empirical relations between the elastic parameters and temperatures of the tested specimens to describe the distortional strain energy density of rock salt under different temperatures and deviation stresses. The results are obtained under temperatures ranging from 273 to 467 Kelvin. The results indicate that the uniaxial compressive strengths (σ_c) of salt decrease linearly with increasing temperature. The tensile strength (σ_B) decreases linearly with increasing specimen temperature as shown in Figure 2.7. The triaxial compressive strength results, under the same confining pressure (σ_3), the maximum principal stress at failure (σ_1) decreases with increasing specimen temperature.

The diagram in Figure 2.8 clearly indicates that the effect of temperature on the salt strength was larger when the salt was under higher confining pressures. When σ_m is below 20 MPa, the octahedral shear strengths for salt were less sensitive to the temperature. The effect of temperature on the salt strength may be enhanced for the salt cavern with high frequency of injection-retrieval cycles. To be conservative the maximum temperature (induced during injection) and the maximum shear stresses (induced during withdrawal) in salt around the cavern should be determined (normally by numerical simulation). The salt stability can be determined by comparing the computed temperature distribution and mechanical and thermal stresses against thecriterion proposed above. The results should lead to a conservative design of the safe maximum and minimum storage pressures.

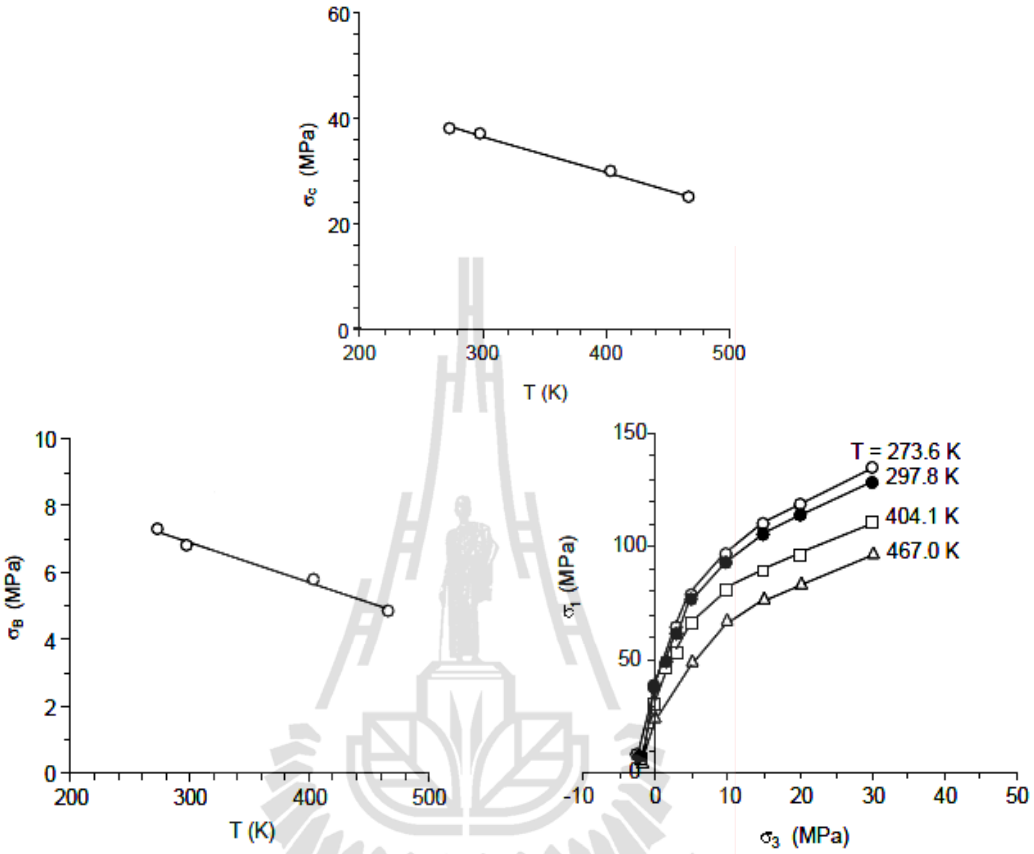

Figure 2.7 (a) Uniaxial compressive strength of salt as a function of temperature.

(b) Brazilian tensile strength of salt as a function of temperature.

(c) Majors principal stress at failure as a function of confining pressure.

(Sriapai et al., 2012)

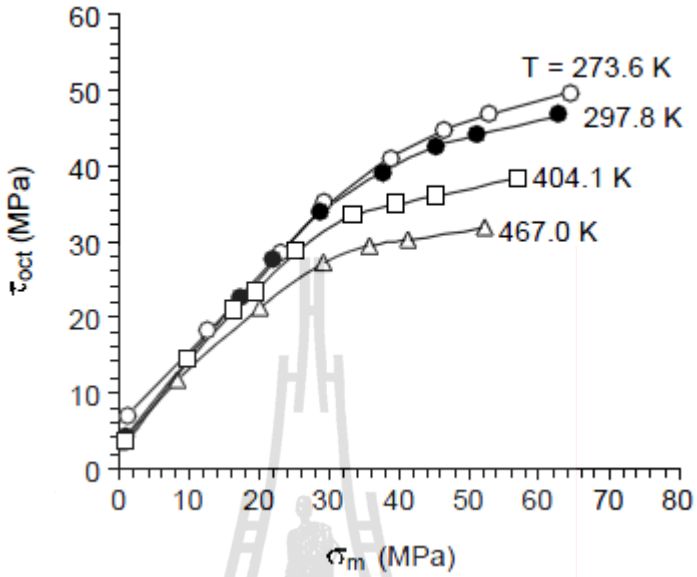

Figure 2.8 Octahedral shear strength of salt as a function of mean stress. (Sriapai et al., 2012)

Khathipphathee and Fuenkajorn (2013) proposed performance assessment of the Maha Sarakham salt for CO_2 storage. The testing temperatures are 273 and 303 K. The tests methods and calculation follow the ASTM (D7070-08) standard practices. The test duration is 21 days. The Exponential creep law is used to describe the time-dependent deformations of the salt specimens. The test results indicate that the creep deformation increases with the temperatures. The test results show that the transient creep under low temperature decreases with time and tends to be constant at steady-state creep phase.

Temperature exerts an effect on deformability and strength of rocks (Vosteen and Schellschmidt, 2003; Shimada and Liu, 2000; Okatov et al., 2003). It has been found that rock strength and elastic properties decrease as the temperature increases. In addition, experimental and theoretical studies on the effect of temperature on rock

salt strength have been rare. Such knowledge is necessary for the design and stability analysis of salt around compressed-air and natural gas storage caverns (Duddeck and Nipp, 1982). During injection period a storage cavern may experience temperatures as high as 140 °C (414 K), depending on the injection rate and the maximum storage volume and pressure (Katz and Lady, 1976; Gronefeld, 1989; Jeremic, 1994).

2.5 Ring Tension Tests

Ripperger and Davids (1947) given the tangential stress (σ_θ) along the loaded diameter of a rock disk with a center hole as;

$$\sigma_\theta = 2Pk_F/\pi Dt \tag{2.4}$$

where P is the applied load, D is the disk diameter, t is the disk thickness, k_F is the stress concentration factor, which is a Fourier function of hole radius (r_i) and disk radius (r_o). The exact solution of the concentration factor, k_F, is

$$k_F = 2(A_0 + 4B_2) - B_0\left(\frac{r_o}{r}\right)^2 + \sum_{n=2,4,\ldots}^{\infty}\left[P_n\left(\frac{r}{r_o}\right)^n + Q_n\left(\frac{r_i}{r}\right)^{n+2}\right] \tag{2.5}$$

where r is the distance from the center. r_o is the disk radius, and r_i is the hole radius. The Fourier coefficients (A, B, etc.) are derived as follows:

$$A_0 = \frac{1}{2(1-\bar{r}^2)} \tag{2.6}$$

$$B_0 = -\frac{\bar{r}^2}{1-\bar{r}^2} \tag{2.7}$$

$$A_n = \frac{1}{2R_n}\left(\frac{1-\bar{r}^{2n}}{n} - \frac{1-\bar{r}^{(2n-2)}}{n+1}\right) \tag{2.8}$$

$$B_n = \frac{1}{2R_n}\left(\frac{1-\bar{r}^{2n}}{n} - \frac{1-\bar{r}^{(2n+2)}}{n-1}\right) \tag{2.9}$$

$$C_n = \frac{\bar{r}^n}{2R_n}\left(-\frac{1-\bar{r}^{2n}}{n} + \frac{1-\bar{r}^{(2n-2)}}{n+1}\cdot\bar{r}^2\right) \tag{2.10}$$

$$D_n = \frac{\bar{r}^n}{2R_n}\left(-\frac{1-\bar{r}^{2n}}{n}\cdot\bar{r}^2 + \frac{1-\bar{r}^{(2n+2)}}{n-1}\right) \tag{2.11}$$

$$R_n = \left(1-\bar{r}^{2n}\right)^2 - n^2\cdot\bar{r}^{(2n-2)}\cdot\left(1-r^2\right)^2 \tag{2.12}$$

$$P_n = 2n(n+1)\cdot(n+2)A_{n+} 2(n+1)\cdot(n+2)^2 B_{(n+2)}\ ;\ n = 2,4,... \tag{2.13}$$

$$Q_n = \left(\frac{2}{\bar{r}^2}\right)\cdot\left[n^2(n+1)C_n + n(n+1)\cdot(n+2)D_{(n+2)}\right];\ n = 2,4,... \tag{2.14}$$

where $\bar{r}$ is relative hole radius (hole radius / disk radius). Since the maximum tensile stress occurs at the hole boundary, the tensile strength (σ_{Ring}) of the rock disk can be calculated by using the k_F value at $r = r_i$. Equation (2.2) can be rewritten as

$$\sigma_{Ring} = 2Pk_F/\pi Dt \tag{2.15}$$

where (σ_{Ring}) is the ring test tensile strength, P_f is the failure load, and K_F is the stress concentration factor at the hole boundary.

An approximate value for the concentration factor, K_F, derived by Hobbs (1964) is

$$K_F = 6 + 38\bar{r}^2 \qquad \text{for } 1.0 > \bar{r} > 0.1 \qquad (2.16)$$

Jaeger and Hoskins (1966) studied the failure of rock materials in the form of rings subjected to line loadings on either their internal or external surfaces is studied. Formulae for the stresses and some numerical values are given. Experimental results for three fine-grained rocks are given and values of the tensile strengths so obtained are compared with those from direct tension, indirect tension (Brazilian) and bending tests. It is found that the calculated tensile stresses at failure for rings loaded in either fashion, and for bending tests, are considerably higher than those for direct tension or the indirect tensile (Brazilian) test. It is suggested that this is due to the fact that in the two latter cases the stresses are uniform (or nearly so) over the section in which failure takes place, while in the three former they vary almost linearly across it. This suggests that a criterion for failure must not simply involve the stresses at a point, but also their rate of change with position.

Hudson (1968) study tensile strength and the ring test. Results of ring tests on a gypsum plaster, with and without limestone inclusions, are presented with the emphasis on small hole sizes. The tensile strength varies within the ring test between two constant values. One is the true tensile strength in this situation for large hole sizes when the elastic calculations adequately represent the physical situation. The other is a totally fictitious tensile strength for small hole sizes which have no effect on failure. Tensile strength variation within the ring test is thus explained by the gradual breakdown of elasticity theory as the hole size is reduced. Tensile strength variation between the ring test and Brazilian test, however, remains a paradox. It is

shown that the latter variation is not caused by ignoring the compressive stress component in the Brazilian biaxial stress field.

Fuenkajorn and Daemen (1986) conducted ring tension tests on 229 mm (9 ins diameter disks of Grande basaltic andesite and Pomona basalt) with various center hole sizes in order to study the relationship between ring tensile strength and relative hole radius (hole radius/disk radius). The tensile strength, σ_R, decreases as the relative hole radius increases. A power equation represent the coefficients of strength and shape, respectively, adequately represents the ring tensile strength as a function of relative hole radius over the range investigated. This equation can be used to distinguish the effect of the hole size from the strength results, to predict the tensile strength of a ring sample containing arbitrary hole sizes, and to approximate the critical relative hole radius of the material tested.

CHAPTER III

SAMPLE PREPARATION

3.1 Sample preparation

The salt specimens are prepared from 100 mm diameter cores drilled from the depths ranging between 70 m and 120 m by Asean Potash Mining Co. in the northeast of Thailand (Figure 3.1). The salt belongs to the Middle Salt member of the Maha Sarakham formation. The cores are drilled and dried-cut to obtain disk specimens with a thickness of 38 mm with a center hole diameter of 31.5 mm (Figures 3.2 and 3.3). Some salt specimens prepared for ring tension testing are shown in Figure 3.4. A total of 20 samples are prepared. Tabakh et al. (1999) and Warren (1999) give detailed descriptions of the salt and geology of the basin. Sample preparation is conducted in laboratory facility at the Suranaree University of Technology. Table 3.1 summarizes the specimen number, depth, dimensions and density. The average density of salt specimens is 2.18±0.06 g/cm^3

3.2 Strain gage installation

Strain gages (TML, Type. PFL-10-11-1L) are installed to measure tensile strains at the inner hole wall where the tensile crack is initiated (Figure 3.5). Gage length is 10 mm. Gage factor is 2.12±1%. The gage installed perpendicular to the loading direction is to measure the tangential tensile strain. The three bond (1786 E) was used to attach strain gage onto specimen surface. The important component of three bonds is the ethyl 2 cyanoacrylate 85% by weight. All strain gages are

connected to the digital strain meter device. Strains are read at each 250 newtons load increment until failure. After preparation the specimens are wrapped with plastic sheet at all time to prevent it from subjecting to the surrounding humidity. No bedding is observed in the specimens.

Figure 3.1 Salt cores drilled from the depth ranging between 70 m and 120 m by Asean Potash Mining Co.

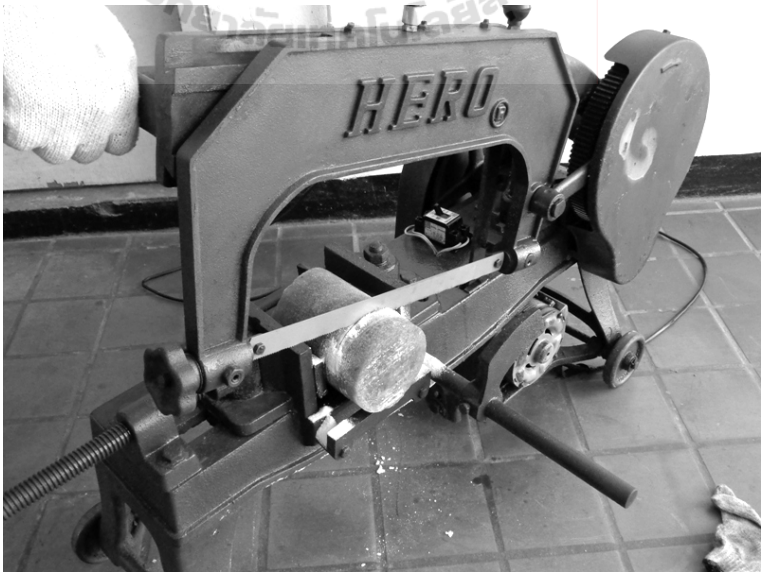

Figure 3.2 Salt core is dry-cut by a cutting saw.

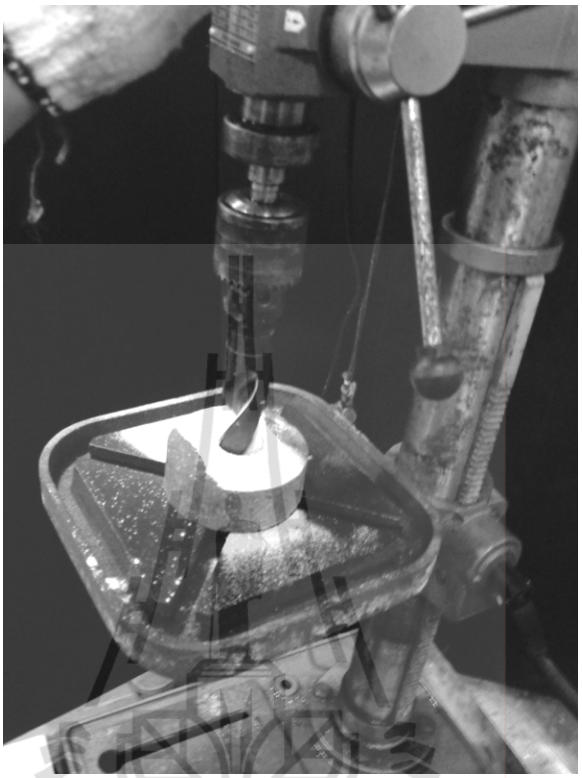

Figure 3.3 Salt specimen is drilled to obtain the center.

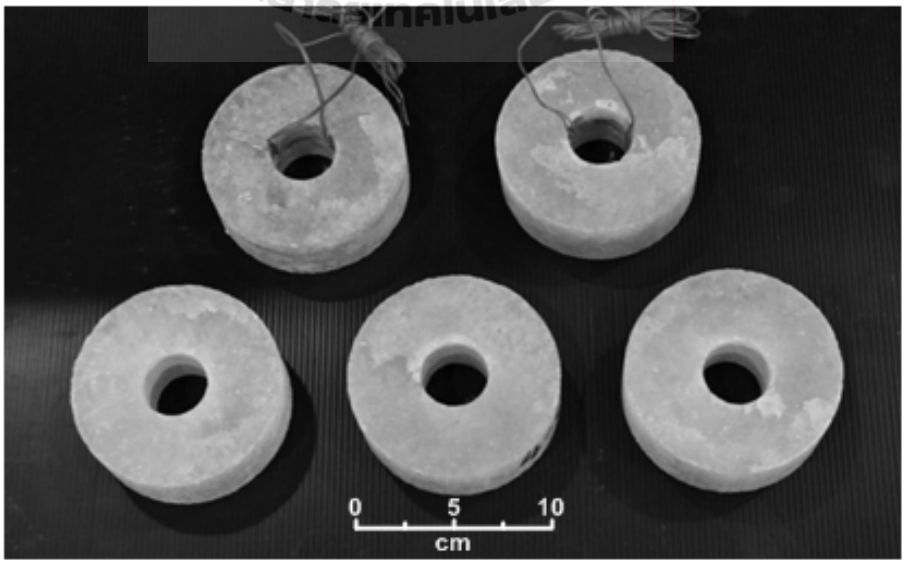

Figure 3.4 Salt specimens prepared for ring tension test.

Table 3.1 Specimen dimensions prepared for ring tension testing.

Specimen No.	Depth (m)	Disk diameter (mm)	Hole diameter (mm)	Thickness (mm)	Density (g/cm^3)
MS-RT-05-05	123.006-123.045	101.09	31.92	38.85	2.21
MS-RT-01-09	82.870-82.909	100.22	32.59	39.02	2.25
MS-RT-06-02	122.850-122.889	100.31	31.76	38.47	2.29
MS-RT-01-11	82.947-82.986	100.88	32.30	39.42	2.21
MS-RT-01-08	82.831-82.870	101.20	32.21	38.70	2.15
MS-RT-04-02	71.033-71.071	100.68	32.05	38.75	2.19
MS-RT-04-04	71.111-71.150	101.00	31.65	38.60	2.13
MS-RT-04-03	71.071-71.111	100.68	31.60	40.13	2.09
MS-RT-04-05	71.150-71.189	100.48	31.77	38.75	2.17
MS-RT-04-10	70.678-70.716	100.50	31.56	38.23	2.17
MS-RT-05-01	73.440-73.480	100.26	31.91	40.33	2.20
MS-RT-06-05	122.729-122.768	100.6	32.07	39.21	2.21
MS-RT-07-01	72.680-72.719	100.59	32.30	38.60	2.22
MS-RT-07-04	72.799-72.838	100.50	32.10	39.40	2.09
MS-RT-01-14	82.599-82.637	101.00	32.10	37.70	2.29
MS-RT-05-06	122.969-123.006	100.93	31.92	36.59	2.21
MS-RT-07-03	72.760-72.799	100.36	31.76	38.93	2.13
MS-RT-01-10	82.909-82.947	100.70	32.10	38.10	2.10
MS-RT-01-07	82.871-82.831	101.12	32.02	39.50	2.14
MS-RT-03-01	77.042-77.082	101.18	32.16	40.23	2.14
Average			2.18±0.06		

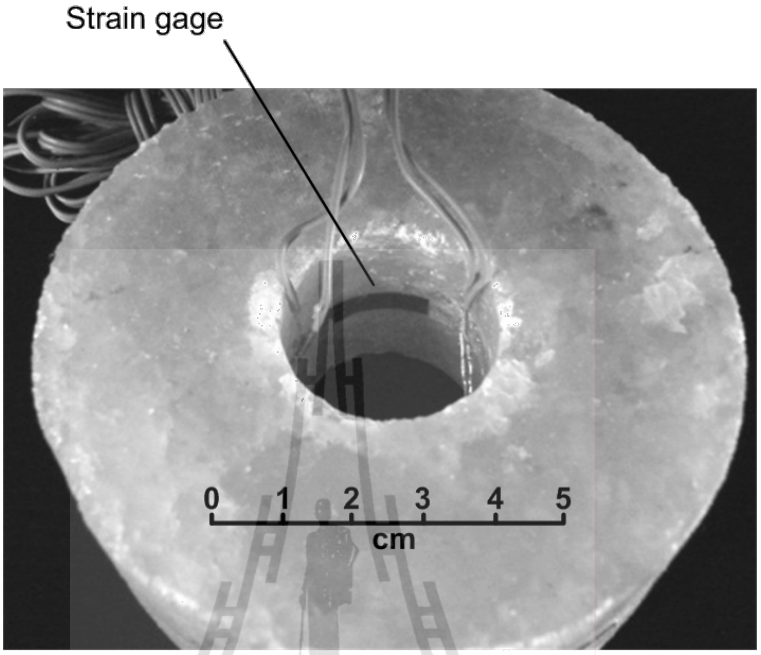

Figure 3.5 Strain gages installed to measure tensile strain at the crack initiation points. The gages length is 10 mm.

CHAPTER IV

COMPUTER SIMULATION

4.1 Objective

The finite difference analysis is performed to compare the stress distribution in the ring test specimen under the diametral loading with the close-form solution described earlier. The distribution of the tangential stress normalized by the applied load P (σ_θ/P) and the normalized radial stress (σ_r/P) along loading diameter will be determined. The model dimensions are identical to the specimen used in the test.

4.2 Model of analysis

The finite difference analyses are used to determine the stress-strain distributions along the loading diameter of the ring test specimen. Shape and dimensions of salt specimen is identical to those used in the test, as shown in Figure 4.1. The model is assigned to be 38 mm thick. The finite difference code FLAC 4.0 (Itasca, 1992) is used in this simulation. Due to the presence of two symmetry planes (horizontal and vertical) across a center of specimen, only one quarter of the specimen needs to be analyzed. The analysis is performed in plane stress. The mesh consists of 400 elements covering an area of 18 cm^2 (1.58 cm inner radius, 5.00 cm outer radius). The finite difference mesh and boundary conditions are designed as shown in Figure 4.2. It is assumed that the salt rock is linearly elastic and isotropic became only the stresses are of interest here. The elastic modulus and Poisson's ratio

of the model are taken as 20 GPa and 0.40 (Fuenkajorn et al., 2012). Material properties used in FLAC simulation are shown in Table 4.1.

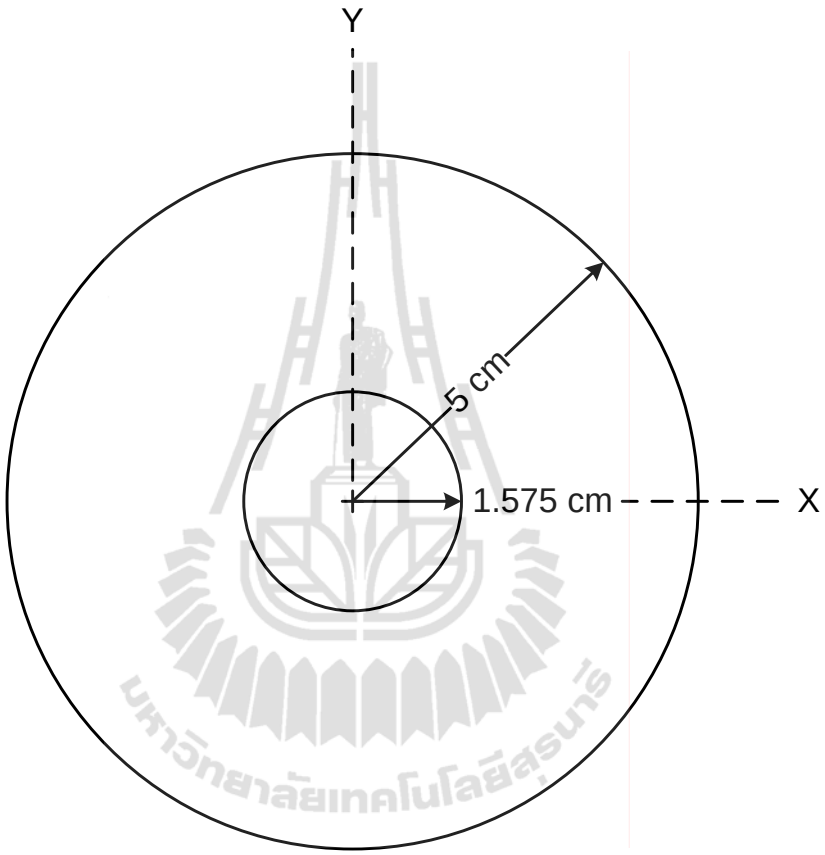

Figure 4.1 Dimensions of specimen used in finite difference analyses.

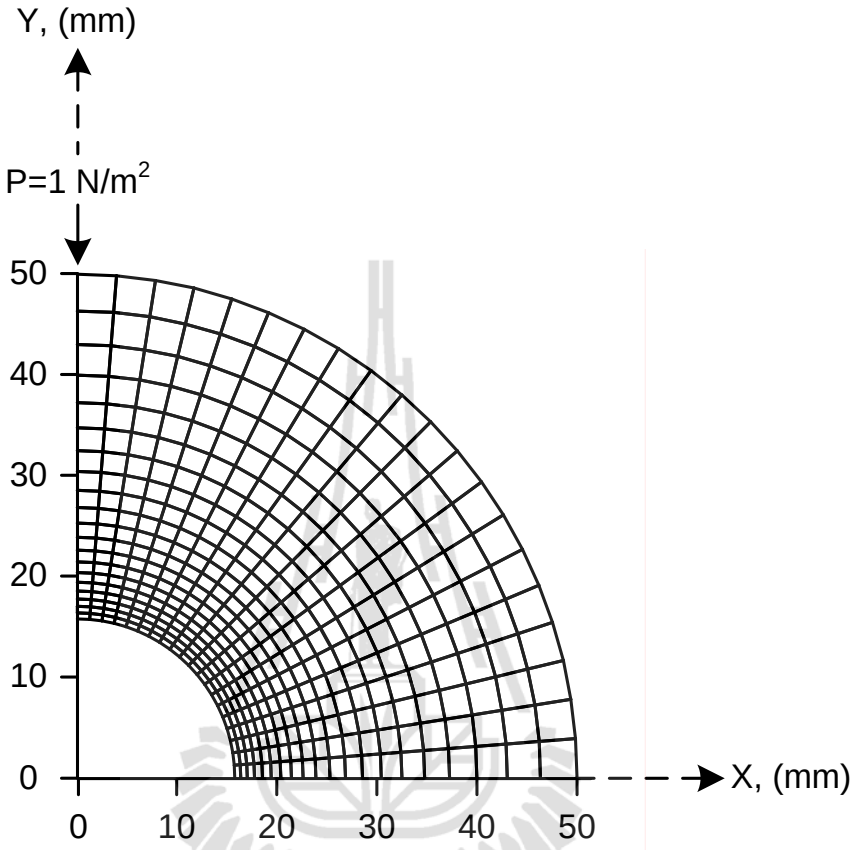

Figure 4.2 Mesh and boundary conditions used for finite difference analysis of ring tension test. It represents the 100 mm disk with 31.5 diameter hole. Arrow (P) indicates the direction of concentrated load.

Table 4.1 Material properties used in FLAC simulation.

Parameter	FLAC	Sources
Elastic modulus, E (GPa)	20.00	Fuenkajorn et al. (2012)
Possion' ration, ν	0.40	Fuenkajorn et al. (2012)
Density, ρ (g/cc)	2.10	Laboratory test
Applied load, (N)	1.00	assumed
Disk diameter, (m)	2.56	Laboratory test
Hole diameter, (m)	0.81	Laboratory test
Thickness, (m)	1.00	Laboratory test

4.3 Results

Figure 4.3 shows the stress vectors of the ring shape specimen model. The maximum tensile stress concentrates at the intersection between the loading diameter and the hole boundary while the maximum compressive stress concentrates at the loading point. Figures 4.4 and 4.5 show the distribution of the normalized maximum and minimum stresses in the specimen. The distribution of the normalized tangential stress (σ_θ/P) and radial stress (σ_r/P) along the loading diameter is plotted as a function of distance from the hole in Figure 4.6. The normalized tangential stress is maximum at the hole boundary. It agrees well with those of the close-form solution. Then the stress slightly decreases and becomes compressive at the loading point. The normalized radial stress is minimum at the hole boundary. It is reduced to zero. Figure 4.7 shows the stress-strain curve at the crack initiation point. The results indicate that the strain increases linearly with increasing stress. This suggests that the nonlinearity observed from the laboratory measurement is primary due to the behavior of the salt. More discussions on this issue are presented in the next chapter.

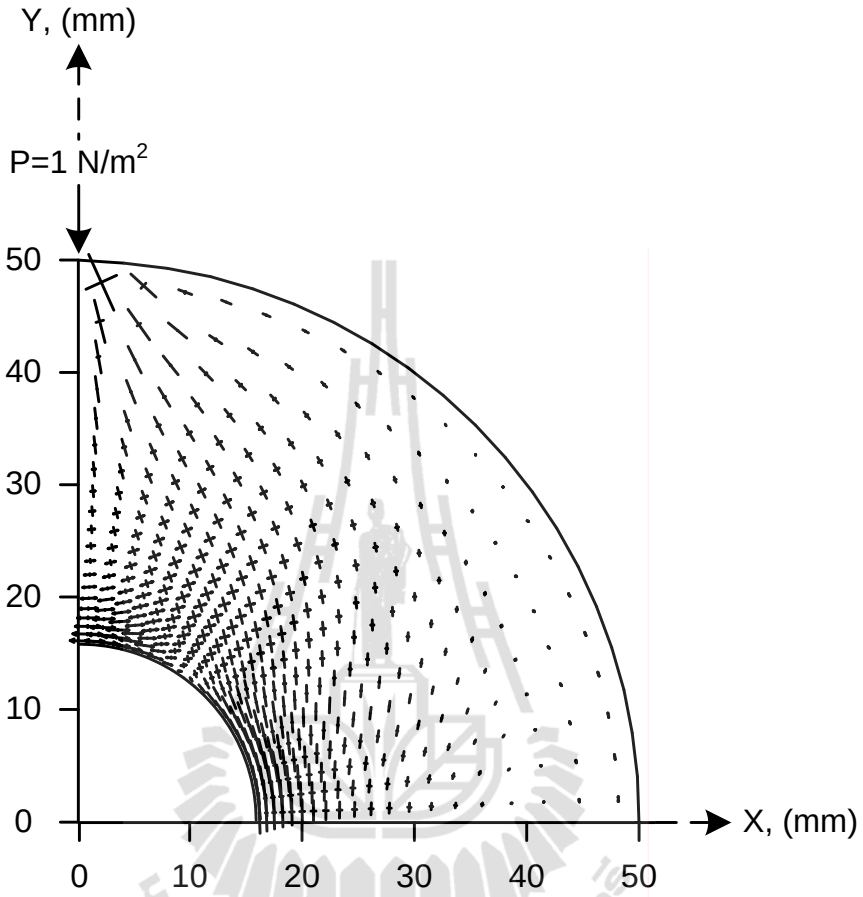

Figure 4.3 Stresses vectors for ring shape specimen models.

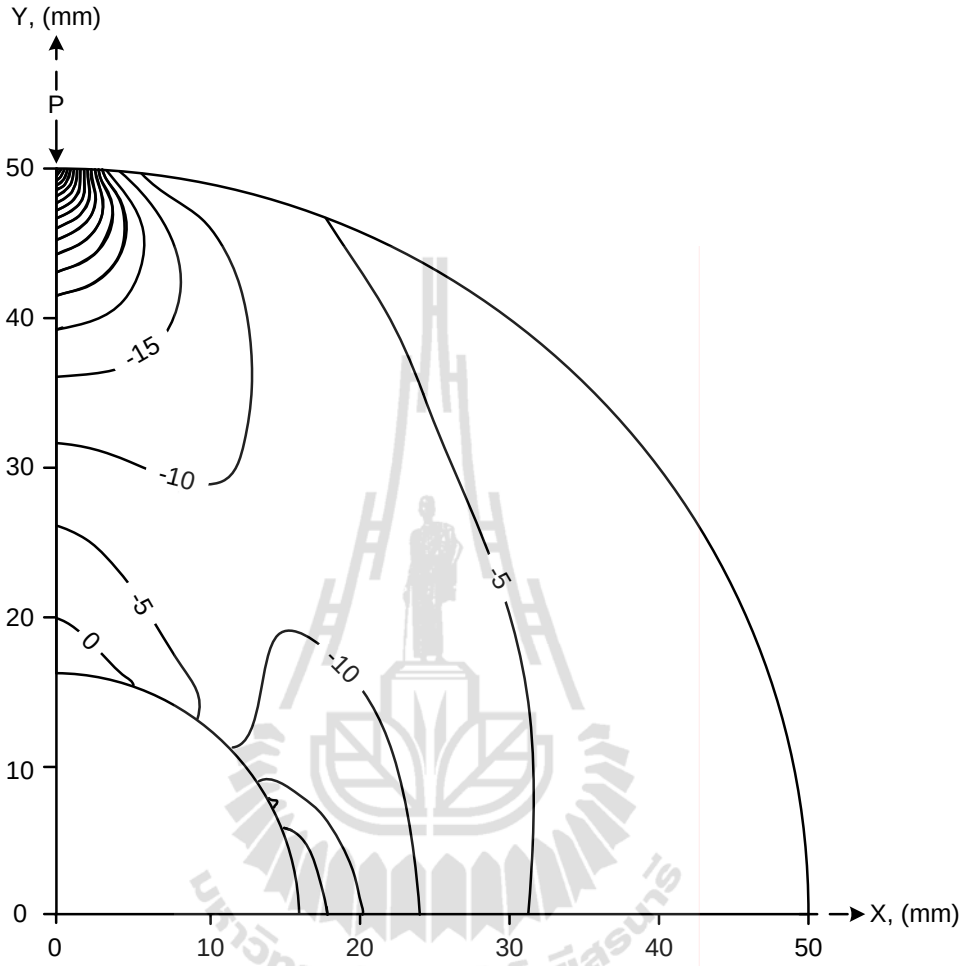

Figure 4.4 Normalized maximum principal stress (σ_1/P) distribution in ring test specimen obtained from finite difference analysis. Arrow indicates the direction of loading. The maximum compressive stress concentrates at the loading point. (inner radius = 1.58 cm, outer radius = 5 cm) P = 1 N. σ_1/P has unit of $1/m^2$.

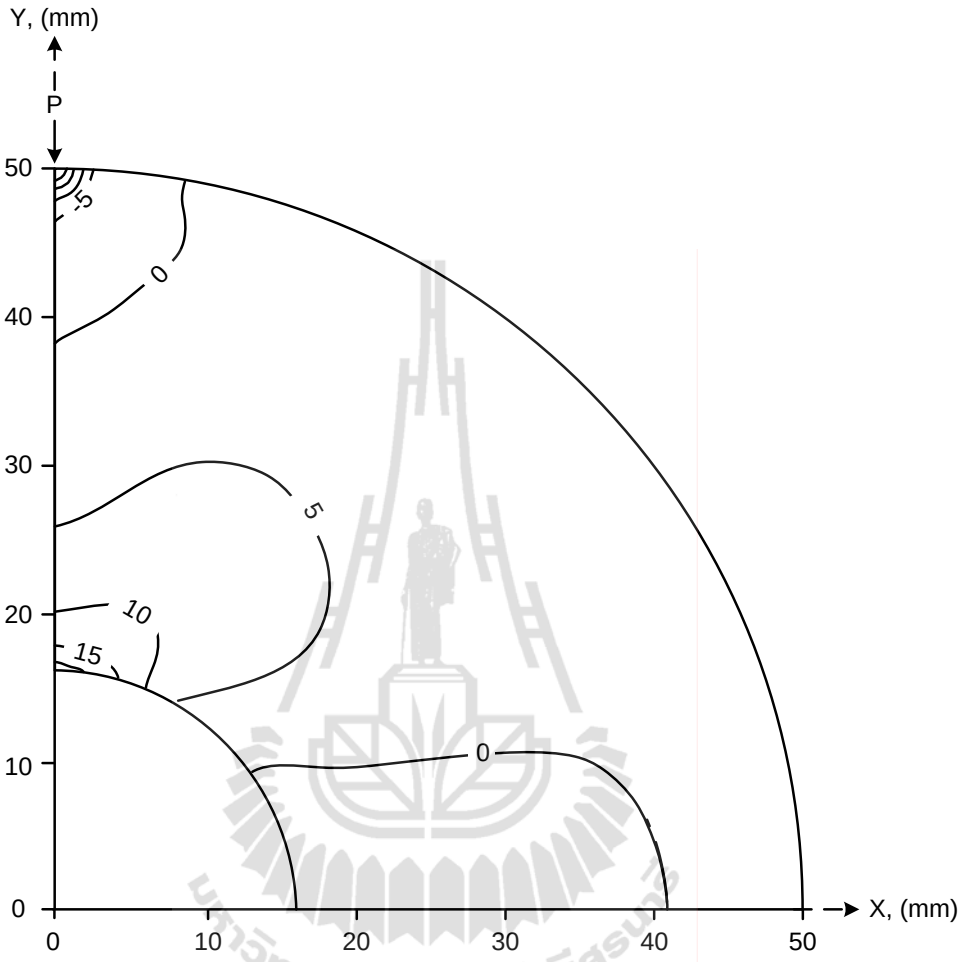

Figure 4.5 Normalized minimum principal stress (σ_2/P) distribution in ring test specimen obtained from finite difference analysis. Arrow indicates the direction of loading. The maximum tensile stress concentrates at the intersection of loading diameter and hole boundary. (inner radius = 1.58 cm, outer radius = 5 cm) P = 1 N. σ_2/P has unit of $1/m^2$.

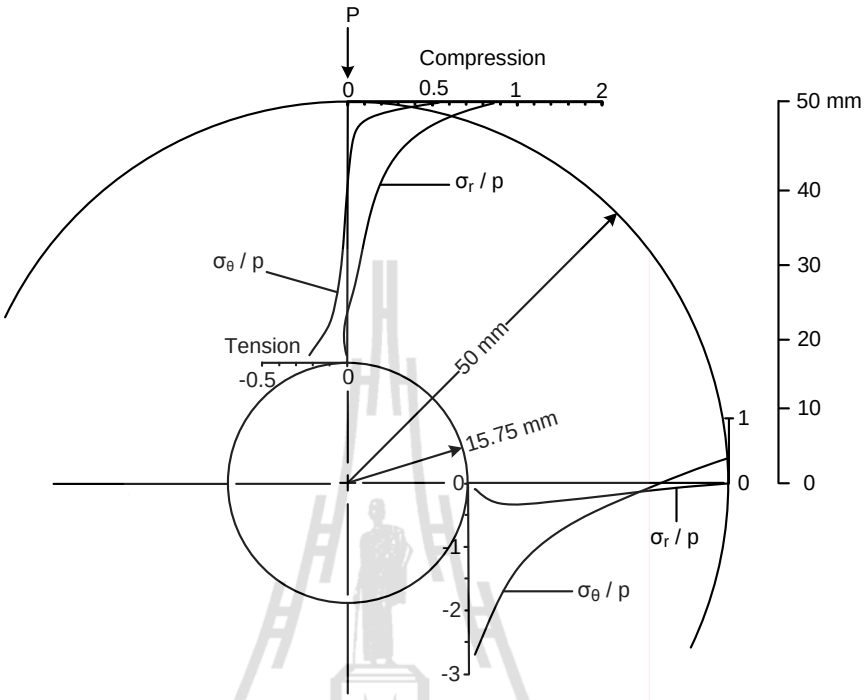

Figure 4.6 Distribution of the normalized tangential stress (σ_θ/P) and radial stress (σ_r/P) along vertical and horizontal stresses obtained from finite difference analysis.

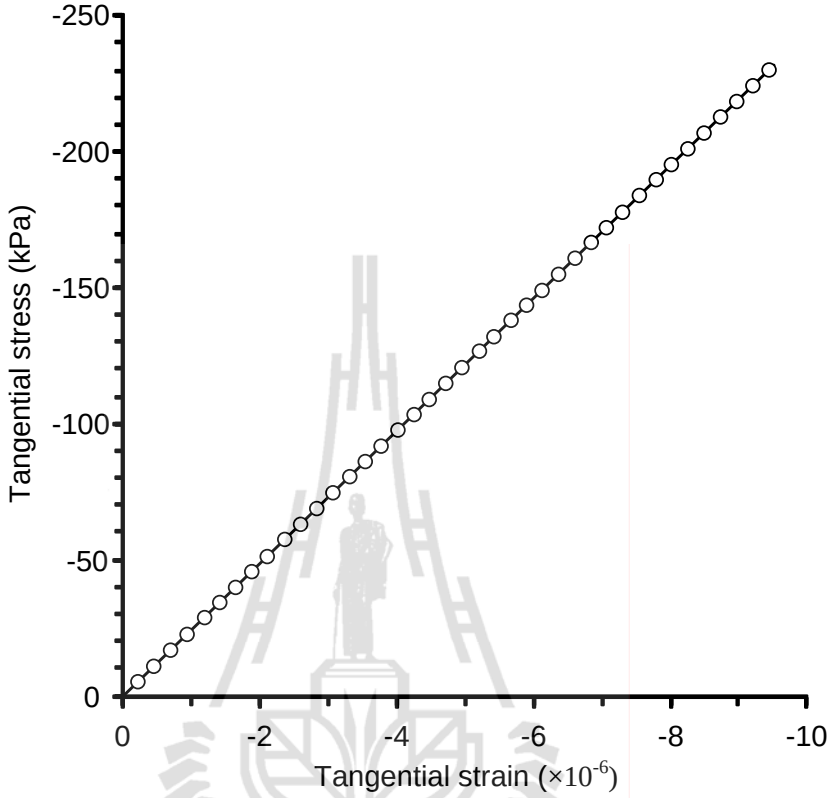

Figure 4.7 Tangential stresses as a function tangential strain at crack initiation point.

CHAPTER V

LABORATORY TESTING

AND TESTING RESULTS

5.1 Introduction

The objective of this section is to experimentally determine the time-dependent of tensile strength of the Maha Sarakham salt under temperatures ranging from 270 to 375 Kelvin. This chapter describes the test method and results.

5.2 Test method

Ring tension test is carried out. The applied loading rates are varied which are equivalent to the tensile stress rates at the crack initiation point from 3×10^{-5} to 3×10^{-1} MPa/s. The digital strain meter indicator (TC-31K) connected with an electronic load cell is used to record the load increment. The load at failure is recorded to determine the salt tensile strength. The specimen deformations are monitored with two strain gages to determine the increase of tensile strains at the inner wall on opposite direction. Photographs are taken of the failed specimens.

5.2.1 Low temperature testing

The salt specimen is placed in the consolidation load frame and installed inside the cooling system for low temperature test at 270 Kelvin. The cooling system is fabricated to test the salt specimen while loading. It can cool the salt specimens down to 270 Kelvin. The cooling system consists of compressor, cool,

coils, hot coils, expansion valve and refrigerant (Figure 5.1). The compressor takes 220-240 volts 50 Hz. The salt specimen is placed in a cooling system for a period of 24 hours before loading. Figure 5.2 shows the specimen placed in the cooling system for low temperature test at 270 Kelvin. The specimen installation, equipment setup and loading are completed within 4 minutes. The changes of specimen temperatures between before and after testing are less than 5 Kelvin. As a result the specimen temperatures are assumed to be uniform and constant with time during the mechanical testing (i.e., isothermal condition).

5.2.2 Ambient temperature testing

For the ring tension testing under ambient temperature (302 Kelvin), the salt specimen is placed in a compression machine and loaded diametrically until failure as shown in Figure 5.3. The electronic load cell is used to record the load increase.

5.2.3 High temperature testing

For the high temperature testing a heating tape with temperature regulator is used to apply constant elevated temperatures to the specimens from 348 to 375 Kelvin. The salt specimens are wrapped with heating tape, foil and insulation while loading as shown in Figure 5.4. A heating tape can heat the salt specimens up to 375 Kelvin. The specimen is installed with the heating system for 24 hours before loading started.

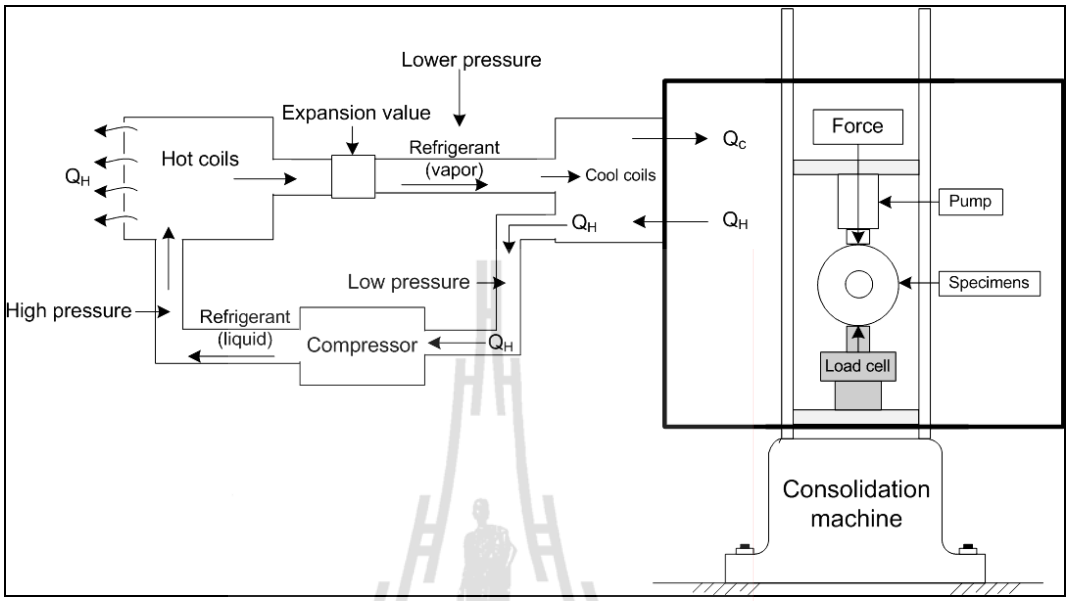

Figure 5.1 Cooling system fabricated for the ring tension test under low temperatures.

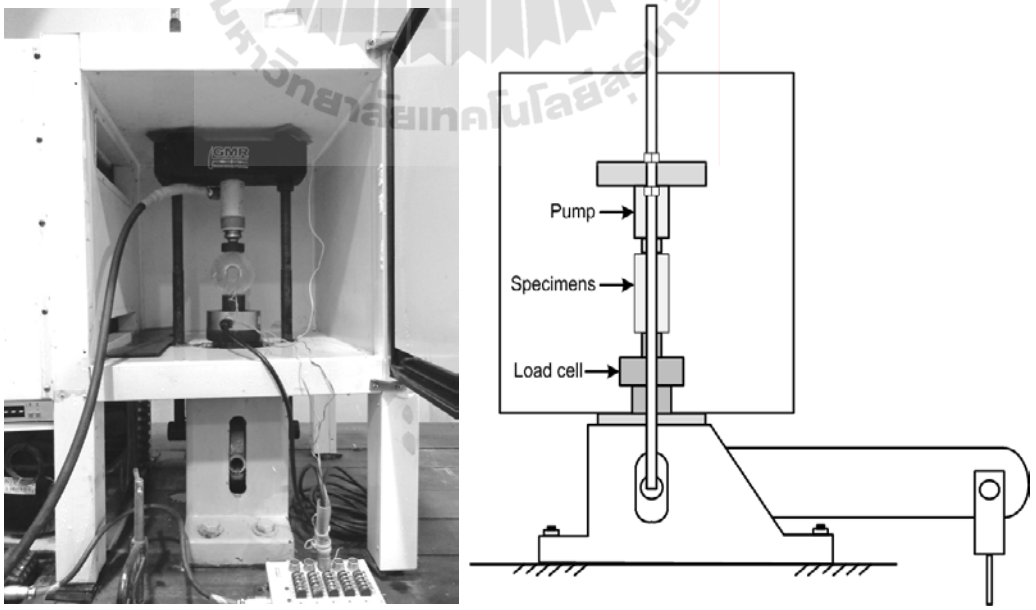

Figure 5.2 A salt specimen placed in the consolidation load frame and inside the cooling system for low temperature test at 270 K.

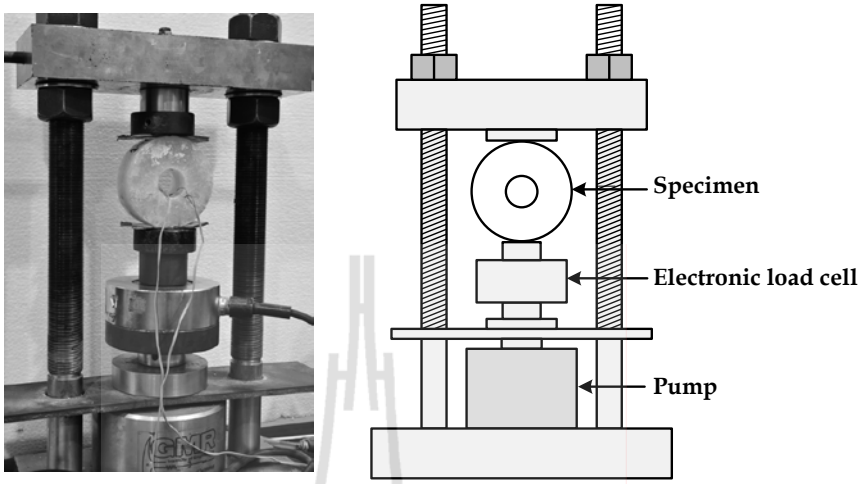

Figure 5.3 Ring tension test on 100 mm disk with 31.5 mm center hole.

Figure 5.4 Salt specimens wrapped with the heating tape and insulator for high temperature testing at 348 and 375 K.

5.3 Tensile strength calculation

The ring tensile strength (σ_{Ring}) can be calculated using the equation (Ripperger and Dvids, 1947):

$$\sigma_{Ring} = \frac{2P_f K_F}{\pi D t} \tag{5.1}$$

where (σ_{Ring}) is the ring test tensile strength, P_f is the failure load, and K_F is the stress concentration factor at the hole boundary. D is the disk diameter and t is the disk thickness.

The stress concentration factor at the hole boundary (K_F) can be calculated using the equation:

$$K_F = 6 + 38\bar{r}^2 \quad \text{for } 1.0 > \bar{r} > 0.1 \tag{5.2}$$

where $\bar{r}$ is relative hole radius (hole radius / disk radius).

5.4 Test results

Figure 5.5 shows some post-test specimens of the Maha Sarakham salt obtained from ring tension testing. Table 5.1 summarizes the strength results. The salt tensile strengths are plotted as a function of stress rate as shown in Figure 5.6. Figure 5.7 shows the tensile stresses as a function of tensile strain for the loading rates of 3×10^{-5}, 3×10^{-4}, 3×10^{-3}, 3×10^{-2} and 0, 3×10^{-1} MPa/s. The results indicate that the tensile strength increases with increasing loading rate and decreases with increasing the temperature (Figure 5.8). Non-linear behavior of the salt is reflected as a curvature of the stress-strain relations.

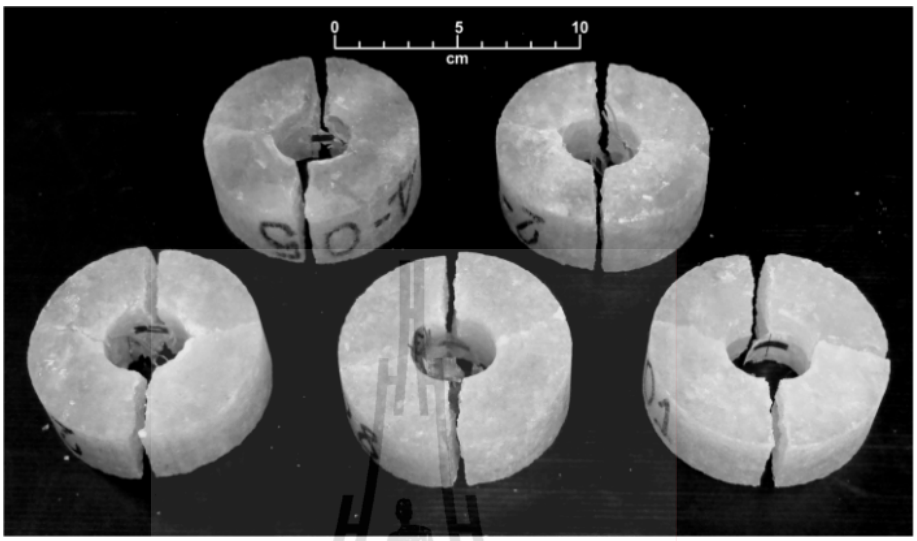

Figure 5.5 Some post-test specimens of the Maha Sarakham salt obtained from ring tension testing.

Table 5.1 Ring tensile strength results.

Stress rates at the crack initiation point, (MPa/s)	**Ring tensile strength, σ_{Ring} (MPa)**			
	Temperature (Kelvin)			
	270±1.29	302±0.46	348±2.09	375±1.76
3×10^{-1}	10.79	10.55	10.27	9.92
3×10^{-2}	10.67	10.23	9.94	9.76
3×10^{-3}	10.20	9.88	9.66	9.39
3×10^{-4}	9.89	9.60	9.35	8.98
3×10^{-5}	9.60	9.28	8.98	8.67

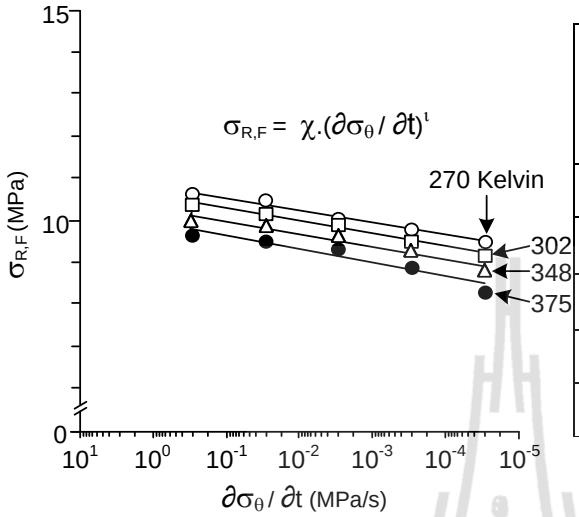

T_{avg} (Kelvin)	$\sigma_{R,F} = \chi\cdot(\partial\sigma_\theta / \partial t)^\iota$		R^2
	χ	ι	
270	11.050	0.0135	0.977
302	10.737	0.0140	0.999
348	10.464	0.0143	0.996
375	10.209	0.0154	0.978
Average	10.615	0.0143	

Figure 5.6 Tensile strength ($\sigma_{R,F}$) as a function of stress rates.

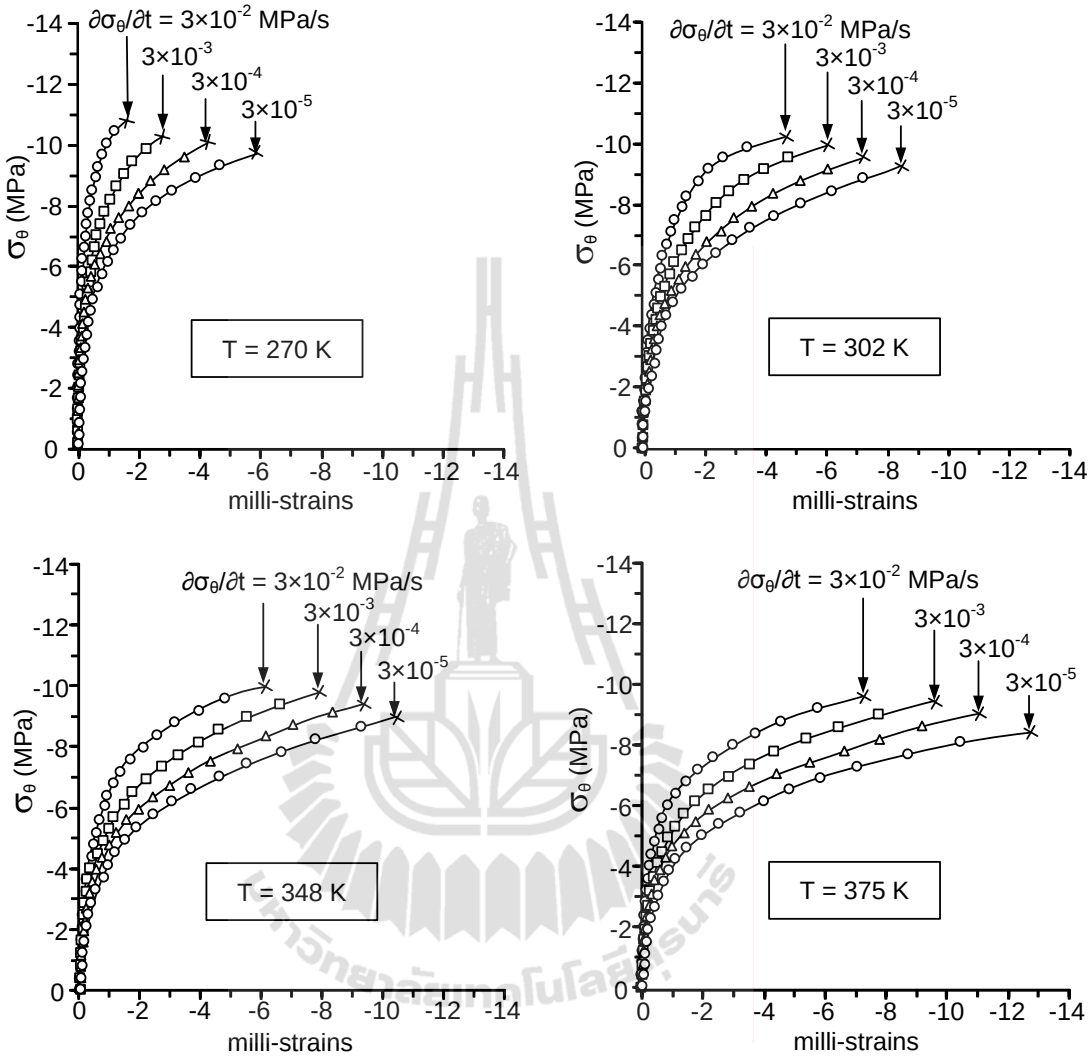

Figure 5.7 Stress-strain curves for various stress rates and temperatures.

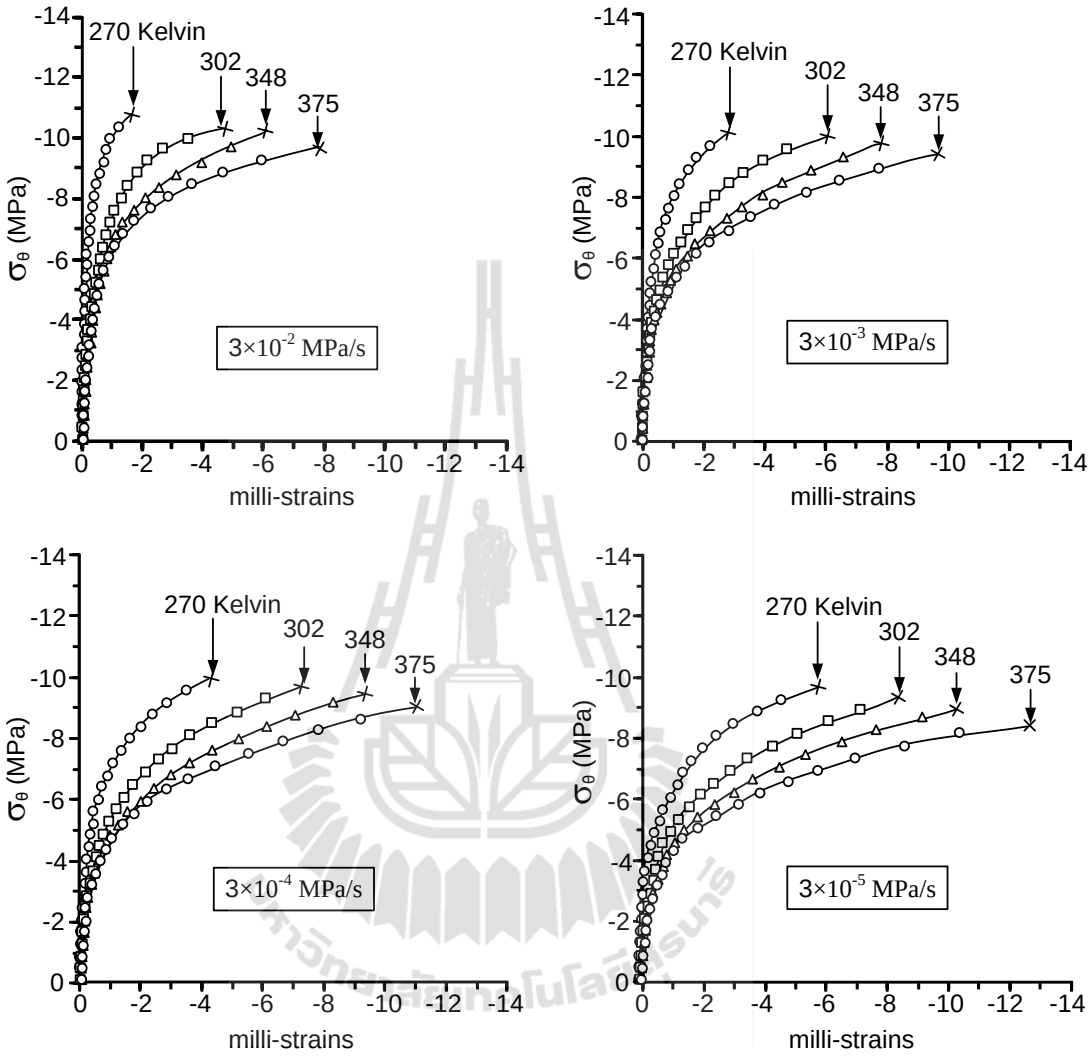

Figure 5.8 Stress-strain curves for different stress rates.

CHAPTER VI

TENSILE CREEP EQUATION AND STRENGTH CRITERION

6.1 Objectives

The purpose of this chapter is to describe the calibration results of the elastic and transient creep parameters. The regression analysis of the proposed tensile creep strain equation with the IBM SPSS Statistics 19 (Wendai, 2000) is performed to determine the elastic and creep parameters. Results from laboratory measurements in terms of the tensile strengths of rock salt under various temperatures and loading rates will also be used to formulate mathematical relations. The objective is to predict the tensile strength under low and elevated temperatures as a function of time.

6.2 Total tensile strain

The total tensile strain at the crack initiation point in specimen ring is divided here in two parts, elastic strain (linear and recoverable strain) and plastic creep strain (time-dependent and non-recoverable strain):

$$\varepsilon_t = \varepsilon_t^e + \varepsilon_t^c \tag{6.1}$$

where ε_t is the total tensile strain, ε_t^e is elastic strain, ε_t^c is plastic creep strains. Since at the crack initiation point the rock is subject to a unidirectional tensile stress, the elastic strain can be calculated as (Jaeger et al., 2007):

$$\varepsilon_t^e = \frac{\sigma_\theta}{E} \tag{6.2}$$

where σ_θ is the tensile stress, E is the tensile elastic modulus. The exponential creep law is used to describe time-dependent strain of the salt. Under isothermal condition the exponential law can describe the creep strain (ε_t^c) as a function of constant stress, constant temperature and time (Senseny, 1983) as follows:

$$\varepsilon_t^c = \alpha \cdot \sigma_\theta^\beta \cdot t^\kappa \cdot \exp(-\lambda/T) \tag{6.3}$$

where α, β, κ and λ are empirical constants, t is elapsed time and T is the constant temperature in Kelvin. Substituting Equations (6.2) through (6.3) into (6.1) we obtain:

$$\varepsilon_t = \frac{\sigma_\theta}{E} + \alpha \cdot \sigma_\theta^\beta \cdot t^\kappa \cdot \exp(-\lambda/T) \tag{6.4}$$

For the stress-rate controlled condition the tensile stress at any loading time (t) can be represented by:

$$\sigma_R = (\partial\sigma_\theta / \partial t) \tag{6.5}$$

$$\text{or } \sigma_\theta = \sigma_R \cdot t \tag{6.6}$$

where σ_R is the constant stress rate (MPa/s) and t is time (second). Assuming that the salt elasticity varies linear with temperature (Archeeploha and Fuenkajorn, 2012):

$$E = -\psi \cdot T + E_0 \tag{6.7}$$

where E_0 is tensile elastic modulus at 0 Kelvin and ψ is the empirical constant. Substituting Equations (6.6) through (6.7) into (6.4) we obtain:

$$\varepsilon_{t\,(t)} = \frac{\sigma_R \cdot t}{\psi \cdot T + E_0} + \alpha \cdot (\sigma_R \cdot t)^{\beta} \cdot t^{\kappa} \cdot \exp(-\lambda/T) \tag{6.8}$$

$$\varepsilon_{t\,(t)} = \frac{\sigma_R \cdot t}{\psi \cdot T + E_0} + \alpha \cdot \sigma_R^{\beta} \cdot t^{\beta+\kappa} \cdot \exp(-\lambda/T) \tag{6.9}$$

Regression analysis of the equation above using the test data is performed to determine the elastic and creep parameters (Table 6.1). Good correlation (R^2 = 0.966) between the constitutive equation and the test data is obtained. Figure 6.1 compares the test data with the back prediction of the proposed equation. This equation can be used to predict the time-dependent tensile deformation of the salt under various constant temperatures. For the Maha Sarakham salt are defined as: ψ = -12.654; E_0 = 15.661 GPa; α = 0.0001; β = 3.442; κ = 0.162; λ = 1724.

6.3 Strength criterion

6.3.1 Tensile strength as a function of time

The salt tensile strengths are plotted as a function of time as shown in Figure 6.2. The results indicate that the tensile strength decreases with increasing time. The empirical equation of these relations can be written as:

$$\sigma_{R,F} = A' \cdot \ln(t) + B' \tag{6.10}$$

where $\sigma_{R,F}$ is the salt tensile strengths (MPa), A' and B' are empirical constants and t is time (second). Figure 6.3 show constants A' and B' are plotted as a function of

temperature. For the Maha Sarakham salt can be empirically defined as a function of temperature (T, in Kelvin), as follows:

$$A' = -0.0126 \cdot T + 13.519 \quad (6.11)$$

$$B' = -6 \times 10^{-5} \cdot T + 0.0153 \quad (6.12)$$

by substituting equation (6.11) and (6.12) into (6.10) the salt tensile strength can be written as a function of time:

$$\sigma_{R,F} = (-0.0126 \cdot T + 13.519) \cdot \ln(t) + (-6 \times 10^{-5} \cdot T + 0.0153) \quad (6.13)$$

This empirical equation may be used to predict the tensile strengths of the salt under various constant temperatures ranging from 270 to 375 and time.

Table 6.1 Parameters calibrated from ring tension test results.

Parameter	**E_0, (GPa)**	**ψ**	**α**	**β**	**κ**	**λ**	**R^2**
Values	15.661	-12.654	0.0001	3.442	0.162	1724	0.966

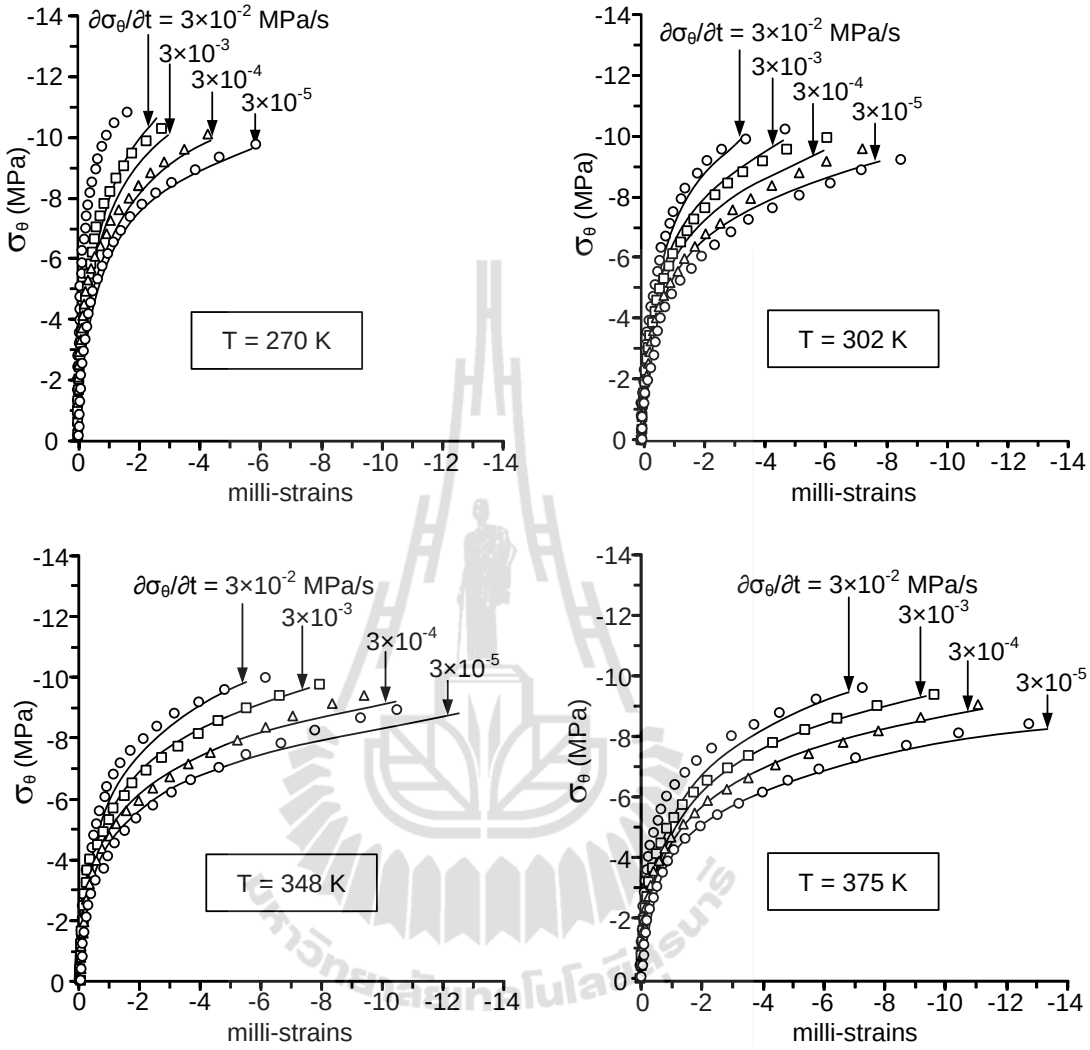

Figure 6.1 Comparisons between test results (points) and back predictions (lines).

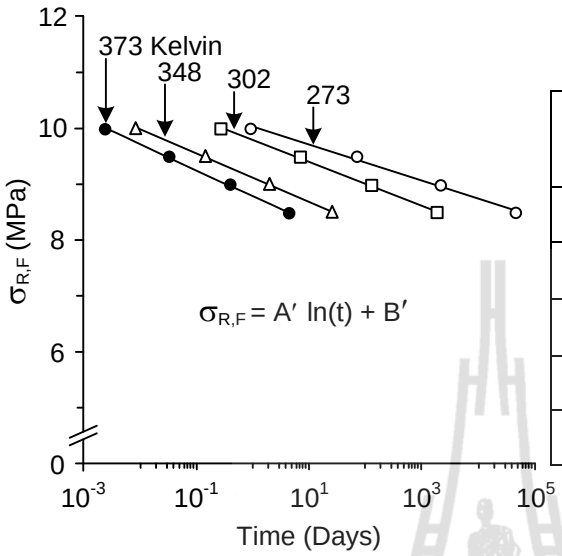

T_{avg} (Kelvin)	$\sigma_{R,F} = A' \cdot \ln(t) + B'$		R^2
	A′	B′	
270	10.023	-0.138	0.994
302	9.797	-0.169	0.998
348	9.122	-0.187	0.999
375	8.804	-0.200	0.999
Average	9.437	0.174	

Figure 6.2 Tensile strength ($\sigma_{R,F}$) as a function of time.

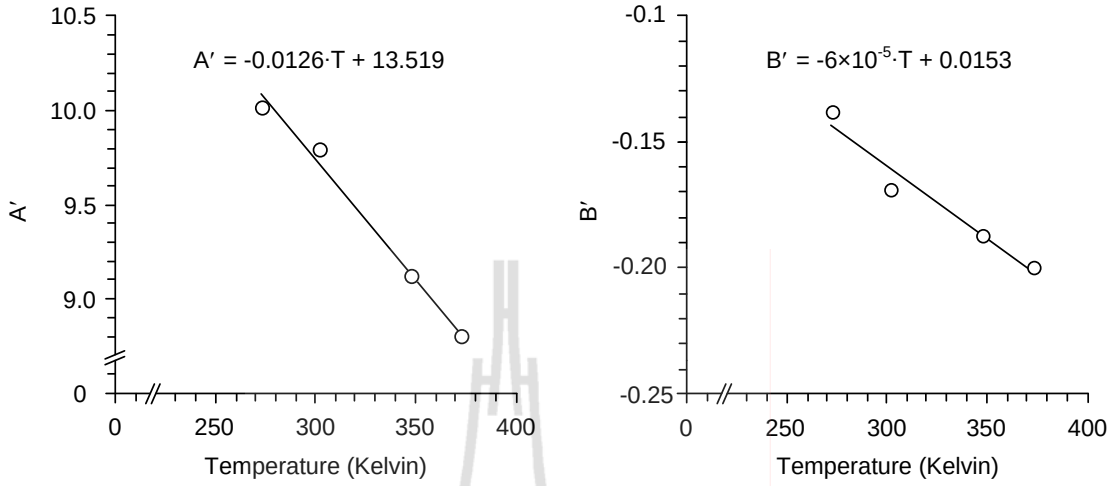

Figure 6.3 Constants A′ and B′ as a function of temperature.

6.3.2 Tensile strength as a function of stress rate

The salt tensile strengths are plotted as a function of stress rate in chapter 5. The results indicate that the tensile strength increases with increasing the loading rate, which can be best represented by a of power equation:

$$\sigma_{R,F} = \chi \cdot (\partial\sigma_\theta/\partial t)^{\iota} \tag{6.14}$$

where $\sigma_{R,F}$ is the salt tensile strengths (MPa), χ and ι are empirical constants. The unit of stress rate $(\partial\sigma_\theta/\partial t)$ is MPa/s. Figure 6.4 show constants χ and ι are plotted as a function of temperature. For the Maha Sarakham salt the parameters in equation (6.14) can be best described by a linear and exponential equation in terms of the temperature, as follows:

$$\chi = -7.7\times10^{-3}\cdot T+13.101 \tag{6.15}$$

$$\iota = 9.9\times10\text{-}^{3}\cdot e^{(0.0011\cdot T)} \tag{6.16}$$

by substituting equations (6.15) and (6.16) into (6.14) the salt tensile strengths can be rewritten as a function of stress rate:

$$\sigma_{R,F} = \left(-7.7\times10^{-3}\cdot T+13.101\right)\cdot\left(\partial\sigma_\theta/\partial t\right)^{\left(9.9\times10^{-3}\right)\cdot e^{(0.0011\cdot T)}} \tag{6.17}$$

This equation may be used to predict the tensile strength of Maha Sarakham salt under various constant temperatures ranging from 270 to 375 Kelvin and loading rates ranging from 3×10^{-1} to 3×10^{-5} MPa/s.

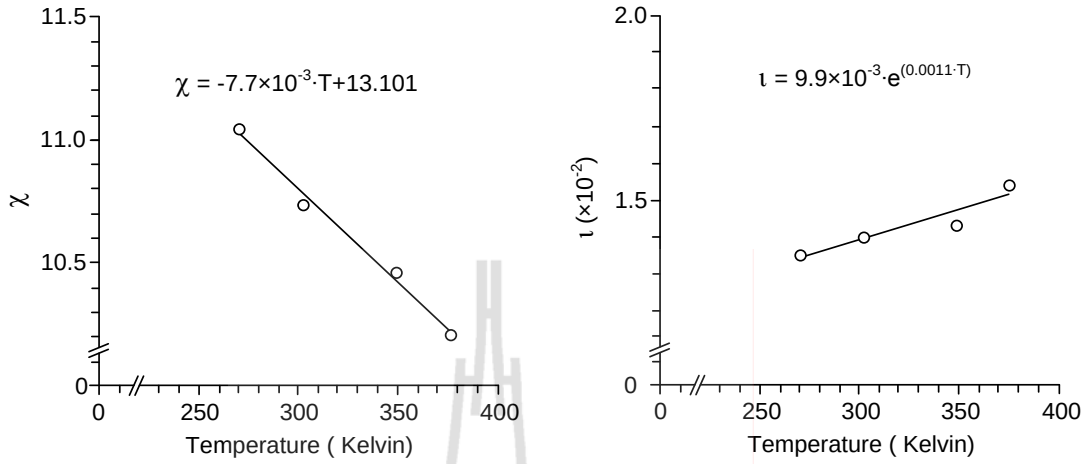

Figure 6.4 Constants χ and ι as a function of temperature.

CHAPTER VII

DISCUSSIONS, CONCLUSIONS AND RECOMMENDATIONS FOR FUTURE STUDIES

7.1 Discussions and conclusions

This study is aimed to experimentally assess the time-dependent tensile strength and deformability of rock salt obtained from the Maha Sarakham formation. A line load is applied along the disk diameter under various the loading rates which are equivalent to the tensile stresses at the crack initiation point ranging from 3×10^{-5} to 3×10^{-1} MPa/s. For the low temperature testing a cooling system is fabricated to test the salt specimen while loading. For the high temperature testing a heating tape with temperature regulator are used to apply constant temperatures to the specimens from 348 to 375 Kelvin.

The ring tensile strength decreases with increasing temperatures. The results agree with the experimental observations by of Sriapia et al. (2012). They study the effect of temperature on compressive and tensile strength of the same salt. It is found here that the tensile strength increases with increasing loading rate, which agrees with the experimental observations by Sang et al. (2003) who studied strain-rate dependency of the dynamic tensile strength of rock.

The time-dependent strain induced in the salt consists of both instantaneous and transient state components. No cleavage sliding observed suggests that no steady-state creep occurs. The tensile cracks are induced at the inter-granular

boundaries rather than cleavage sliding (dislocation climb rather than dislocation glide). This agrees with the observation by Fuenkajorn and Daemen (1988). The creep strain increases with temperature under all loading rates. At the crack initiation point of ring specimen, salt is subjected to unidirectional tensile stress. Close form solutions [equation (5.1) through (5.2)] agree well with the results from the computer simulation. The tensile strength equation can predict the time-dependent tensile deformation of the salt under various constant temperatures.

The ring tension test on rock salt is similar to the in-situ condition of the mine roof and thus the results from this study may be more suitable than those from the Brazilian tension test. It seems reasonable that the derive loading rate dependent equations for deformability and strength are transferable to other salt under tensile load such as mine roof, cavern roof and tunnel roof. Limitations exist with regard to the application of these equations to long term salt storage cavern. Here, both deformability and strength are under only transient creep phases and thus the proposed equations for steady-state creep phases or long term strength may not be applicable. The findings can be used to estimate the time-dependent tensile strength of salt roof under various isothermal temperatures, such as those around waste storage openings.

7.2 Recommendations for future studies

The assessment of predictive capability of the proposed ring tension testing technique has been limited to rock of Maha Sarakham salt. Verification of the ring tension test proposed concept should be tested under a wider range of salt from other sources. The test specimens here are relatively small. Testing on larger specimens is

desirable. Strictly speaking the stress conditions in the mine roof would be similar to the beam bending test. As results the repeated assessment of the time-dependency of the salt strength and deformability should be performed by beam bending test as well.

REFERENCES

Allemandou, X. and Dusseault, M. B. (1996). Procedures for cyclic creep testing of salt rock, results and discussions. In **Proceedings of the Third Conference on the Mechanical Behavior of Salt** (pp. 207-218). Clausthal-Zellerfeld: Trans Tech Publications.

Archeeploha, S. and Fuenkajorn, K. (2012). Thermal effects on strength and deformability of Maha Sarakham salt. In **Proceedings of the Second Southern Hemisphere Symposium SHIRMS 2012** (pp. 47-61). May 15-17, Sun City, Pilansberg, South Africa.

Arieli, A., Heard, H. C. and Mukherjee, A. K. (1982). Deformation modeling in sodium chloride intermediate and elevated temperatures. In R. W. Rohde and J. L. Swearengen (eds). **Mechanical Testing for Deformation Model Development** (pp. 342-365). Philadelphia: ASTM Spec. Technical Publications.

ASTM D2664-95a. Standard test method for triaxial compressive strength of undrained rock core specimens without pore pressure measurements. In **Annual Book of ASTM Standards** (Vol. 04.08). Philadelphia: American Society for Testing and Materials.

ASTM D2938-95. Standard test method for unconfined compressive strength of intact rock core specimens. In **Annual Book of ASTM Standards** (Vol. 04.08). Philadelphia: American Society for Testing and Materials.

ASTM D3967-95a. Standard test method for splitting tensile strength of intact rock core specimens. In **Annual Book of ASTM Standards** (Vol. 04.08). Philadelphia: American Society for Testing and Materials.

ASTM Standard D7070. (2008). Standard practice for creep of rock core under constant stress and temperature. In **Annual Book of ASTM Standards**, West Conshohocken, PA.

Carter, B. J. and Hansen, F. D. (1983). Creep of rocksalt: a review. **Tectonophysics** 92: 275-333.

Charpentier, J-P. (1984). Creep of rock salt elevated temperature. In **Proceedings of the Second Conference on the Mechanics Behavior of Salt** (pp. 131-136). Clausthal, Germany: Trans Tech Publications.

Cristescu, N. and Hunsche, U. (1996). A comprehensive constitutive equation for rock salt determination and application. In **Proceedings of the Third Conference on the Mechanical Behavior of Salt** (pp. 191-205). Clausthal-Zellerfeld, Germany: Trans Tech Publications.

Duddeck, H. W. and Nipp, H. K. (1982). Time and temperature dependent stress and displacement fields in salt domes. In **Proceedings of the 23rd Symposium on Rock Mechanics** (pp. 596-603). Berkeley, New York Publications: AIME.

Fokker, P. A. (1998). The micro-mechanics of creep in rock salt. In **Proceedings of the Fourth Conference on the Mechanical Behavior of Salt** (pp. 49-61). Clausthal-Zellerfeld, Germany: Trans Tech Publications.

Franssen, R. C. M. and Spiers, C. J. (1990). Deformation of polycrystalline salt in compression and in shear at 250-350°C. **Deformation Mechanisms,**

Rheology and Tectonics, Geological Society Special Publication 45: 201-213.

Fuenkajorn, K. and Daemen, J. J. K. (1986). Shape Effect on Ring Test Tensile Strength: Key to Energy Production. In **Proceedings of the 27th U.S. Symposium on Rock Mechanics** (pp. 155-163). June 23-25, Tuscaloosa: University of Alabama,

Fuenkajorn, K. and Daemen, J. J. K. (1988). Boreholes closure in salt. **Technical Report Prepared for The U.S. Nuclear Regulatory Commission, Report No. NUREG/CR-5243 RW.** University of Arizona.

Fuenkajorn, K. and Klanphumeesri, S. (2010). Direct tension tests of intact rock using compression-to-tension load convertor. **Research and Development Journal of the Engineering Institute of Thailand** 21(2): 51-57.

Fuenkajorn, K., Sriapai, T. and Samsri, P. (2012). Effects of loading rate on strength and deformability of Maha Sarakham salt. **Engineering Geology** 135-136: 10-23.

Gronefeld, P. (1989). Thermodynamic behavior of HP natural gas caverns in salt—Theoretical calculations and practical experience. In **Proceedings of the International Conference on Storage of Gases in Rock Caverns** (pp. 121-127). Trondheim, Rotterdam: A. A. Balkema.

Hamami, M., Tijani, S. M. and Vouille, G. (1996). A methodology for the identification of rock salt behavior using multi-steps creep tests. In **Proceedings of the Third Conference on the Mechanical Behavior of Salt** (pp. 53-66). Clausthal-Zellerfeld: Trans Tech Publications.

Hansen, F. D. (1984). Physical and mechanical variability of natural rock salt. In **Proceedings of the Second Conference on the Mechanical Behavior of Salt** (pp. 23-39). Clausthal-Zellerfeld: Trans Tech Publications.

Hobbs, D. W. (1964). The tensile strength of rocks. **International Journal of Rock Mechanics and Mining Sciences** 1(3): 385-394.

Hudson, J. A. (1968). Tensile strength and the ring test. **International Journal of Rock Mechanics and Mining Sciences** 6: 91-97.

Itasca. (1992). **User Manual for FLAC-Fast Langrangian Analysis of Continua, Version 4.0.** Itasca Consulting Group Inc., Minneapolis, Minnesota.

Jacker, J. C. and Hoskins, E. R. (1966). Stresses and failure in ring of rock loaded in diametral tension or compression. **British Journal of Applied Physics** 17: 685-692.

Jaeger, J. C., Cook, N. G. W. and Zimmerman, R.W. (2007). **Fundamentals of Rock Mechanics Fourth Edition** (500 pp.). Blackwell publishing, Oxford.

Jeremic, K. L. (1994). **Rock Mechanics in Salt Mining** (530 pp.). Rotherdam: A. A. Balkema.

Katz, D. L. V. and Lady, E.R. (1976). **Compressed Air Storage for Electric Power Generation** (224 pp.). Malloy Lithograhing Inc., Michigan.

Kenkhunthod, N. and Fuenkajorn, K. (2010). Influence of loading rate on deformability and compressive strength of three Thai sandstones. **Geotechnical and Geological Engineering** 28(5): 707-715.

Kensakoo, T., Phueakphum, D. and Fuenkajorn, K. (2007). Mechanical properties of Maha Sarakham salt as affected by inclusions. In **Rock Mechanics**

Proceedings of the First Thailand Rock Mechanics Symposium (pp. 103-119). September 13-14, Greenery Resort, Nakhon Ratchasima, Thailand.

Khathipphathee, T. and Fuenkajorn, K. (2013). Performance assessment of Maha Sarakham salt for CO_2 storage. In **Proceedings of the Fourth Thailand Symposium on Rock Mechanics** (pp. 111-119.). January 24-25, Im Poo Hill Resort, Nakhon Ratchasima, Thailand.

Kumar, A. (1968). The effect of stress rate and temperature on the strength of basalt and granite. **Geophysics** 33(3): 501-510.

Liang, W. G., Xu, S. G. and Zhao, Y. S. (2006). Experimental study of temperature effects on physical and mechanical characteristics of salt rock. **Rock Mechanics and Rock Engineering** 39(5): 469-482.

Liang, W. G., Zhao, Y. S., Xu, S. G. and Dusseault, M. B. (2010). Effect of strain rate on the mechanical properties of salt rock. **International Journal of Rock Mechanics and Mining Sciences** 48: 161-167.

Ma, L. and Daemen, J. J. K. (2006). Strain rate dependent strength and stress-strain characteristics of a welded tuff. **Bulletin of Engineering Geology and the Environment** 65(3): 221-230.

Okatov, R. P., Nizametdinov, F. K., Tsai, B. N. and Bondarenko, T. T. (2003). Time and temperature factors in construction of rock strength criteria. **Journal of Mining Science** 39(2): 139–142.

Pudewills, A. (1995). **Thermal Simulation of Drift Emplacement: Temperature Analyses.** Topical Report, Forschungszentrum Karlsruhe.

Raj, S. V., and Pharr, G. M. (1992). Effect of temperature on the formation of creep substructure in sodium chloride single crystal. **American Ceramic Society** 75(2): 347-352.

Ray, S. K., Srakar, M. and Singh, T. N. (1999). Effect of cyclic loading and strain rate on the mechanical behaviour of sandstone. **International Journal of Rock Mechanics and Mining Sciences** 36: 543-549.

Ripperger, E. A. and Davids, N. (1947). Critical stresses in a circular ring. **Transactions of the American Society of Civil Engineering** 112(2308): 619-627.

Sang, H. C., Yuji, O. and Katsuhiko, K. (2003). Strain-rate dependency of the dynamic tensile strength of rock. **International Journal of Rock Mechanics and Mining Sciences** 40(5): 763-777.

Sangha, C. M. and Dhir, R. K. (1972). Influence of time on the strength, deformation and fracture properties of a lower Devonian sandstone. **International Journal of Rock Mechanics and Mining Sciences** 9: 343-354.

Senseny, P. E. (1983). **Review of Constitutive Laws used to Describe the Creep of Salt** (45 pp.). Battelle Memorial Institute, Columbus, Ohio.

Senseny, P. E. (1984). Specimen size and history effects on creep of salt. In **Proceedings of the First Conference on the Mechanics Behavior of Salt** (pp. 369-379). Clausthal-Zellerfeld: Trans Tech Publications.

Senseny, P. E., Handin, J. W., Hansen, F. D. and Russell, J. E. (1992). Mechanical behavior of rock salt: phenomenology and micro-mechanisms. **International Journal of Rock Mechanics and Mining Sciences** 29(4): 363-37.

Shimada, M. and Liu, J. (2000). Temperature dependence of strength of rock under high confining pressure. **Annuals Disaster Prevention Research Institute** 43B-1: 75–84.

Sriapai. T., Chaowarin, W. and Fuenkajorn, K. (2012). Effects of temperature on compressive and tensile strengths of salt. **ScienceAsia** 38: 166-174.

Tabakh, EL. M., Ultha-Aroon, C. and Schreiber, B. C. (1999). Sedimentology of the cretaceous Maha Sarakham evaporates in the Khorat plateau of northeastern Thailand. **Sedimentary Geology** 123: 31-62.

Varo, L. and Passaris, E. K. S. (1977). The role of water in the creep properties of halite. In **Proceeding of the conference on Rock Engineering** (pp. 85-100). University of Newcastle upon Tyne. England.

Vosteen, H. and Schellschmidt, R. (2003). Influence of temperature on thermal conductivity, thermal capacity and thermal diffusivity for different types of rock. **Physics and Chemistry of the Earth** 28: 499–509.

Warren, J. (1999). **Evaporites: Their Evolution and Economics** (pp.235-239). Blackwell Science, Oxford.

Wendai, L. (2000). Regression analysis, linear regression and probit regression In 13 chapters. **SPSS for Windows: statistical analysis**. Publishing House of Electronics Industry. Beijing.

Yanan, G., Feng, G., Zhang, Z. and Zhang, T. (2010). Visco-elastic-plastic model of deep underground rock affected by temperature and humidity. **Mining Science and Technology** 20(2): 183-187.

APPENDIX A

PUBLICATION

Publication

Wisetsaen, S and Fuenkajorn, K. (2013). Time-dependent tensile strength of Maha Sarakham salt. In **Proceedings of the Fourth Thailand Symposium on Rock Mechanics** (pp. 121-132). January 24-25, Im Poo Hill Resort, Nakhon Ratchasima, Thailand, pp. 121-132.

Rock Mechanics, Fuenkajorn & Phien-wej (eds) © 2013

tensile strength of Maha Sarakham salt

Time-dependent

kajorn

S. Wisetsaen & K. Fuenl

Geomechanics Research Unit, Suranaree University of Technology, Thaila

ngth

Keywords: Rock salt, creep behavior, thermal effect, loading rate, tensile stre

time-dependent

ABSTRACT: The objective of this study is to experimentally assess the

bility of rock salt obtained from the Maha Sarakham formation. tensile strength and deformal
ut to obtain cylinder shaped specimens with a thickness of 38 The drilled cores are dried-c
100 mm and center hole diameter is 31.5 mm. A line load in mm. The disk diameter is
ter under various the loading rates which are equivalent to the applied along the disk diame
initiation point of 0.00003, 0.0003, 0.003, 0.03 and 0.3 MPa/s. tensile stresses at the crack

dicate that the
ith increasing
of salt under

The testing temperatures are varied from 269 to 375 Kelvin. The results in
tensile strength increases with increasing loading rate, and decreases w
temperatures. Exponential law can well describe the time-dependent behavio
tension.

1 INTRODUCTION

lity of rock salt is an important parameter used in the design
rground structures. The rock tensile strength dictates the
ground openings, the maximum internal pressure of unlined

Tensile strength and deformabi
and stability analysis of unde
maximum roof span of underg

nkajorn &
oncentrated
1980; Liang
der low and

storage caverns and the borehole pressure for hydraulic fracturing (Fue
Klanphumeesri, 2010). The effect of temperatures on rock salt has been largely c
on the time-dependent creep deformation under compression (Carter & Hansen,
et al., 2006). Study on the time-dependent effect on the salt tensile strength un
elevated temperatures has been very rare.

determine the time-dependent tensile strength of the Maha
ranging from 269 to 375 Kelvin (0–100 Celsius). The ring
the time-dependent tensile behavior of the salt at the crack

The objective of this study is to
Sarakham salt under temperatures
tension test is performed to assess

[redacted]

N **2 SAMPLE PREPARATIC**

d from 100 mm salt cores drilled from the depth ranging an Potash Mining Co. in the northeast of Thailand. The salt

[redacted]

salts are cores belong to the Middle salt member of the Maha Sarakham formation. The tested Over 30 virtually pure halite, with the anhydrite and clay inclusions of less than 2-3%. ecimens specimens are prepared and tested. The drilled cores are dried-cut to obtain disk sp ough the with a thickness of 38 mm. A center hole with a diameter of 31.5 mm is drilled thro he inner center of the specimen (Figure 1). Strain gages are installed to obtain tensile strain at t

[redacted]

ed (Figure 2). After preparation the specimens are hole wall where the tensile crack is initiat to prevent it from subjecting to the surrounding wrapped with plastic sheet at all time specimens. humidity. No bedding is observed in the

3 TEST METHOD

[redacted]

The salt specimen is placed in a compression machine and loaded diametrically until failure (Figure 3). A concentrated load (point load) technique has been used with the loading rates of 0.00002, 0.0002, 0.002, 0.02 and 0.2 kN/s. The load at failure is recorded to determine the salt tensile strength. The specimens deformations are monitored with two strain gages to

[redacted]

aphs are taken of the failed specimens. For determine the increase of tensile strains. Photogr fabricated to test the salt cylindrical sample the low temperature testing a cooling system is specimens down to 273K. For the high while loading (Figure 4). It can cool the salt ature regulator are used to apply constant temperature testing a heating tape with temper 8 to 375 Kelvin. The salt specimens are elevated temperature to the specimens from 34

[redacted]

ted temperature to the specimens from 348 to 375 Kelvin. The salt specimens are eleva ped with heating tape, foil and insulation while loading (Figure 5). wrap

TENSILE STRENGTH CALCULATION **4**

[redacted]

along the loaded diameter of a rock Ripperger & davids (1947) give the tangential stress (σ_θ) disk with a center hole as;

$$(1) \qquad \sigma_\theta = \frac{2Pk_F}{\pi Dt}$$

[redacted]

e applied load, D is the disk diameter, t is the disk thickness, k_F is the stress where P is th factor, which is a Fourier function of hole radius (r_i) and disk radius (r_o). The concentration of the concentration factor, k_F, is exact solution

[redacted]

$$(2) \qquad k_F = 2(A_0 + 4B_2) - B_0\left(\frac{r_o}{r}\right)^2 + \sum_{n=2,4}^{\infty} \left[P_n\left(\frac{r}{r_o}\right)^n + Q_n\left(\frac{r_i}{r}\right)^{n+2} \right.$$

lt specimens prepared for ring tension test.

Figure 1. Some sa

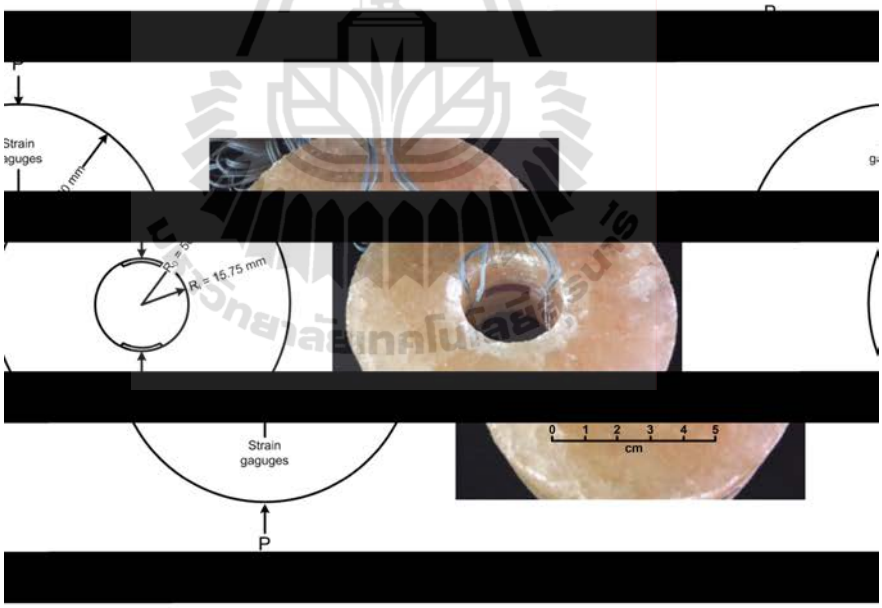

tion points.

Figure 2. Strain gages installed to measure tensile strain at the crack initia
The gages length is 10 mm.

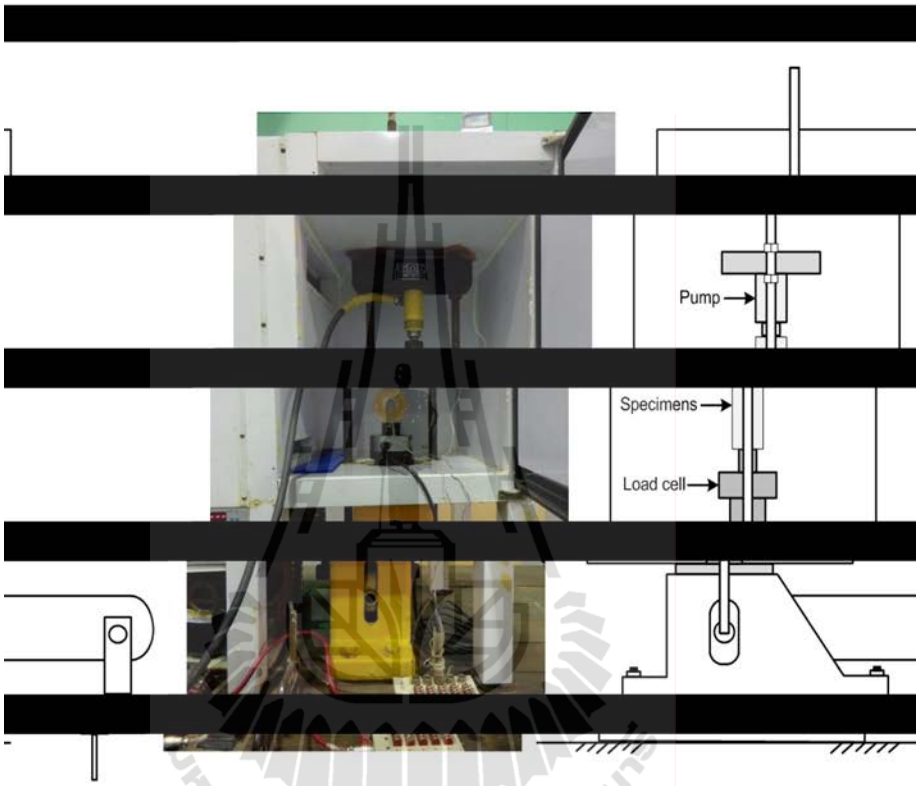

oling system Figure 4. Salt specimen placed in the consolidation load frame and inside the co
for low temperature test at 273 K.

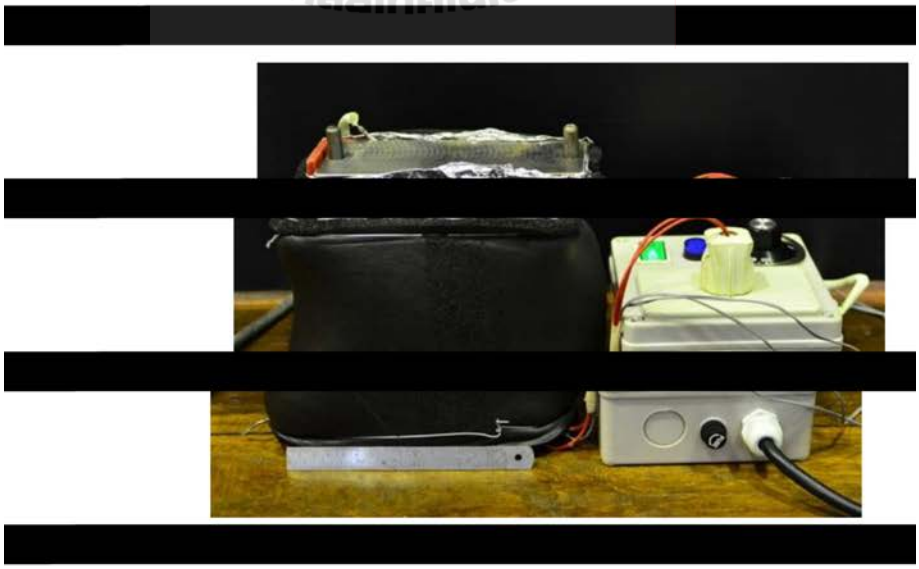

·e Figure 5. Salt specimen wrapped with the heating tape and insulator for high temperatu
testing at 348 and 373 K.

[redacted]

$$B_n = \frac{1}{2R_n}\left(\frac{1-\bar{r}^{2n}}{n} - \frac{1-\bar{r}^{(2n+2)}}{n-1}\right) \quad (6)$$

[redacted]

$$C_n = \frac{\bar{r}^n}{2R_n}\left(-\frac{1-\bar{r}^{2n}}{n} + \frac{1-\bar{r}^{(2n-2)}}{n+1}\cdot\bar{r}^2\right) \quad (7)$$

[redacted]

$$\cdot\bar{r}^2 + \frac{}{n-1}\Bigg) \quad (8) \quad D_n = \frac{}{2R_n}\left(-\frac{}{n}\right.$$

$$\cdot\bar{r}^{(2n-2)}\cdot\left(1-r^2\right)^2 \quad (9) \quad R_n = \left(1-\bar{r}^{2n}\right)^2 - n^2$$

[redacted]

$$)^2 B_{(n+2)}\ ; n = 2,4,... \quad (10) \quad P_n = 2n(n+1)\cdot(n+2)A_{n+} 2(n+1)\cdot(n+2)$$

$$2)D_{(n-2)}\Big]\ ; n = 2,4 \quad (11) \quad Q_n = \left(\frac{2}{\bar{r}^2}\right)\cdot\left[n^2(n+1)C_{n+} n(n+1)\cdot(n+1)\right.$$

[redacted]

e the maximum tensile stress ock disk can be calculated by

where $\bar{r}$ is relative hole radius (hole radius / disk radius). Sinc occurs at the hole boundary, the tensile strength (σ_{Ring}) of the rc using the k_F value at $r = \bar{r}$. Equation (1) can be rewritten as

[redacted]

$$\sigma_{Ring} = \frac{2P_f K_F}{\pi Dt} \quad (12)$$

[redacted]

g) is the ring test tensile strength, P_f is the failure load, and K_F is the stress on factor at the hole boundary. An approximate value for the concentration factor, d by Hobbs (1964) is

where (σ_{Rin} concentrati K_F, derive

[redacted]

$$K_F = 6 + 38\bar{r}^{} \quad \text{for } 1.0 > \bar{r} > 0.1 \quad (13)$$

AC 4.0) is used to confirm the stress distribution of the ring l loading. The model dimensions are identical is those used ribution of the normalized tangential stress (σ_θ/P) and radial

The finite difference method (FL test specimen under the diametra in the test. The results of the dist

[redacted]

inite difference analysis is shown in are shown in Table 1.The simulation 3).

stress (σ_r/P) along loading diameter obtained from f Figure 6. Material properties used in FLAC simulation results agree well with the solution given in Equation (1

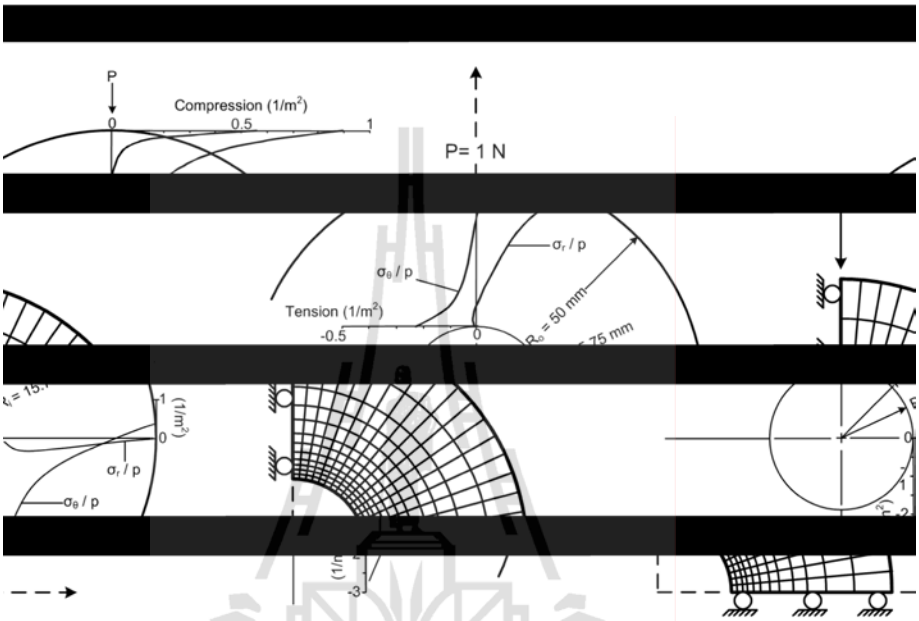

l stresses (σ_θ/P) and radial stresses (σ_r/P) along vertical and

Figure 6. Normalized tangentia

horizontal stresses obtained from finite different analysis.

Table 1. Material properties used in FLAC simulation.

Parameter		FLAC	Equation
20.00	20.00	Elastic modulus, E (GPa)	
0.40	0.40	Possion' ration, ν	
2.10	2.10	Density, ρ (g/cc)	
1.00	1.00	Applied load, (N)	
[illegible]	[illegible]	[illegible]	
ter, (m)	2.56	2.56	Disk diame
ter, (m)	0.81	0.81	Hole diame
m)	1.00	1.00	Thickness,
	9.77	9.77	K_F
strength, σ_{Ring} (MPa)	2.23	2.43	Ring tensile

Table 2. Ring tensile strength results.

ng tensile strength, σ_{Ring} (MPa)	Sample No.	Temperature (Kelvin)	Stress rates at the crack initiation point, (MPa/s)	Ri
[illegible]	[illegible]	[illegible]	[illegible]	[illegible]
0.3	10.72		5-05	
0.03	10.59		1-09	
0.003	10.10		6-02	270±1.29

Rock Mechanics, Fuenkajorn & Phien-wej (eds) © 2013

ults (continue).

Table 2. Ring tensile strength res

e	Stress rates at the crack initiation point, (MPa/s)	Ring tensile strength, σ_{Ring} (MPa)		Sample No.	Temperatur (Kelvin)
	0.3	10.07		5-01	
	0.03	9.94		6-05	
	0.003	9.75		7-01	346±2.09
	0.0003	9.35		7-04	
	0.00003	8.88		1-14	
	0.3	9.72		5-06	
	.03	9.58		7-03	0
	)03	9.39		1-10	376±1.76 0.0
	)03	8.98		1-07	0.0
	8.38	3-01			0.00003

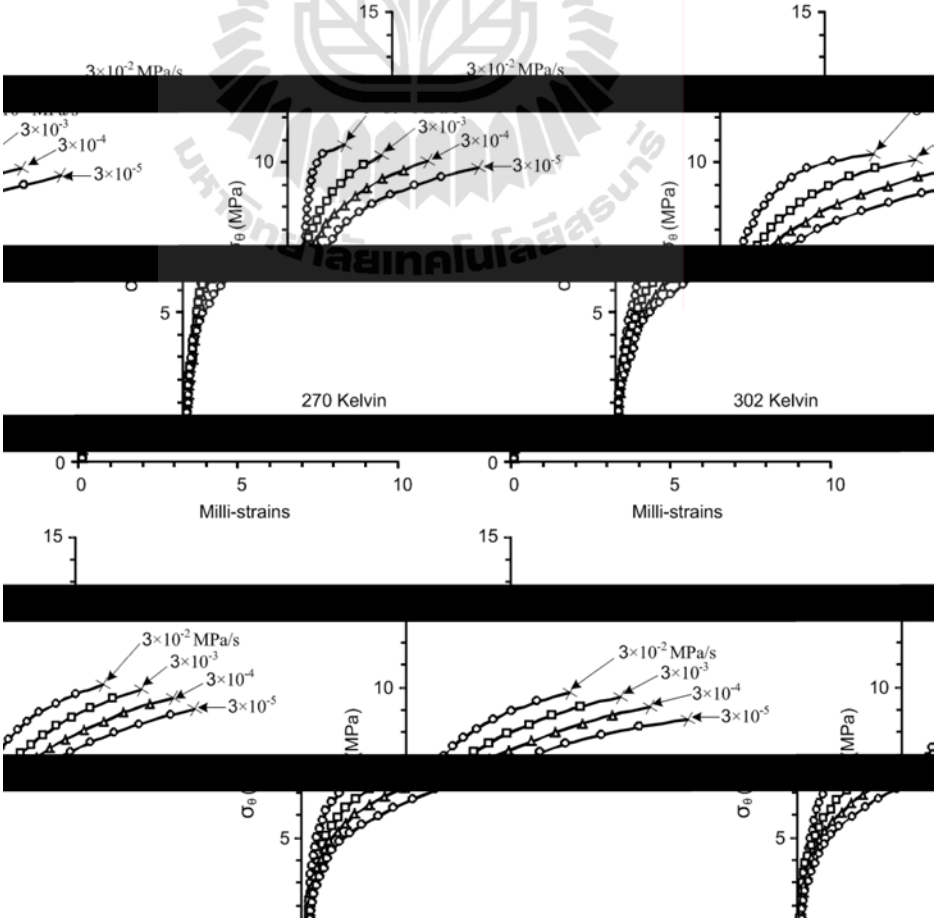

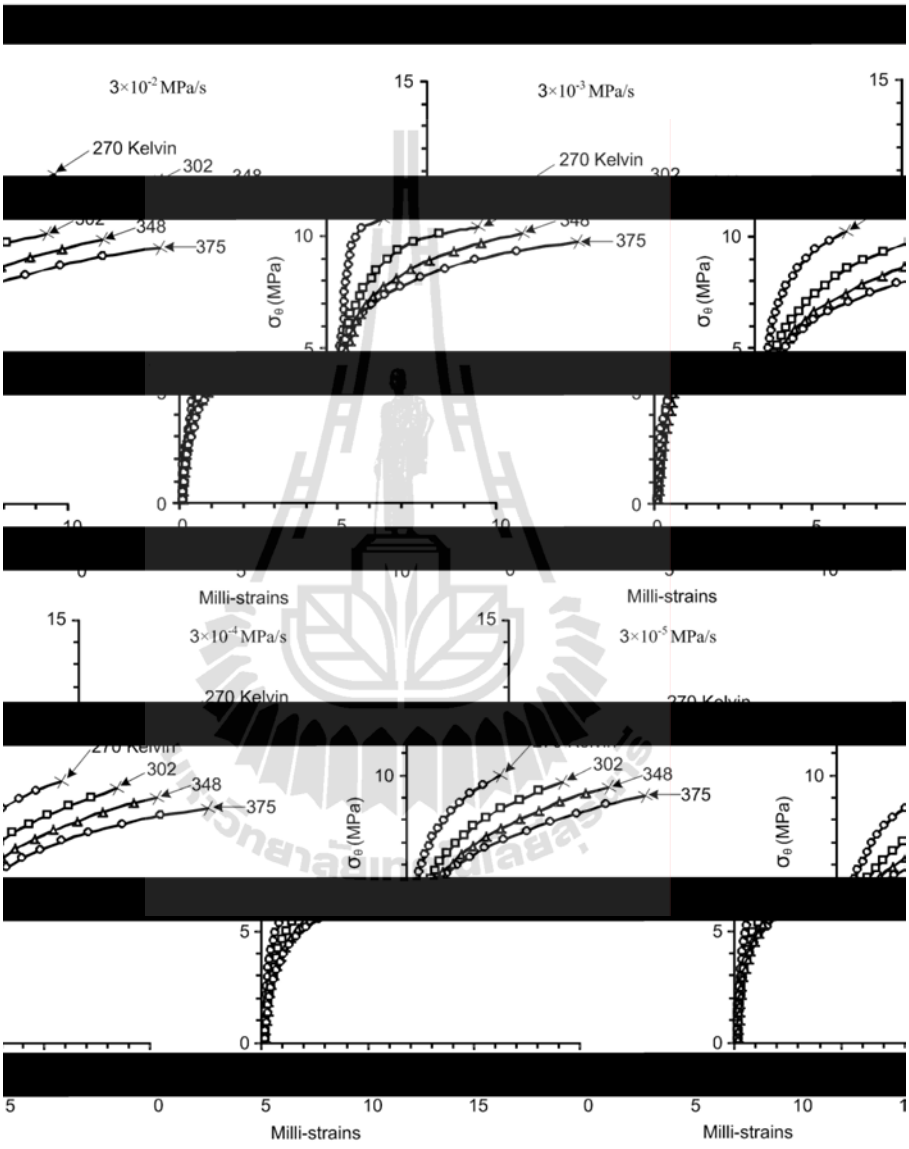

Figure 8. Stress-strain curves for different stress rates.

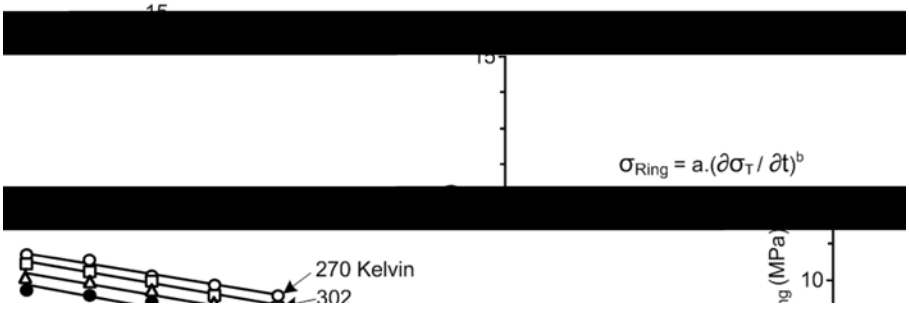

Rock Mechanics, Fuenkajorn & Phien-wej (eds) © 2013

6 TENSILE CREEP MODEL

ı salt ring is divided in two parts, elastic tic creep strain (time-dependent and nonrecoverable strain):

The total tensile strain at the crack initiation point i strain (linear and recoverable strain) and plas

$$\varepsilon_t = \varepsilon_t^e + \varepsilon_t^c \quad (14)$$

ensile strain, ε_t^e is elastic strain, ε_t^c is plastic creep strains, The elastic m the current stress state using classical elastic theory.

where ε_t is the total t strain is calculated fro

$$\varepsilon_t^e = \frac{\sigma_t}{E} \quad (15)$$

strain, E is the tensile elastic modulus. tress at any loading time (t) can be

where σ_t is the tensile stress, ε_t^e is the elastic tensile For the strain-rate controlled condition the tensile s represented by:

$$\sigma_t = \frac{\partial \sigma_t}{\partial t} \cdot t \quad (16)$$

$$\text{or } \sigma_t = \sigma_R \cdot t \quad (17)$$

t strain rate (in MPa/s) and t is time (in second).

where σ_R is the constan

lied to describe the time-dependent behavior of salt. The law in ture. The exponential law presents constant temperatures in function of

Exponential law is app derived by linking the creep strain to stress and tempera the creep behavior of salt as a function of constant stress, time (Senseny, 1983).

$$\varepsilon_t^c = \alpha \cdot \sigma_t^{\beta} \cdot t^{\kappa} \cdot \exp\left(\frac{-\lambda}{T}\right) \quad (18)$$

ure where α is stress constant, β is the stress exponent, κ is time exponent, λ is temperat constant, and T is the absolute temperature.

sticity varies linear with temperature (Archeeploha & Fuenkajorn, 2012):

Assuming that the salt ela

(20) $$\varepsilon_t = \frac{\sigma_R \cdot t}{-\psi \cdot T + E_0} + \alpha \cdot \sigma_R^{\beta} \cdot t^{\kappa} \cdot \exp\left(\frac{-\lambda}{T}\right)$$

ıine the elastic and Regression analysis of the equation above using the test data to determ

ep parameters (Table 3). Good correlation (R^2) between the constitutive equation and the cre
data is obtained. Figure 10 compares the test data with the back prediction of the test
posed equation. This equation can be used to predict the time-dependent tensile pro
ormation of the salt under various constant temperatures. def

7 CONCLUTIONS

erimentally assess the time-dependent tensile strength and This study is aimed to exp
tained from the Maha Sarakham formation. A line load is deformability of rock salt ob
r under various the loading rates which are equivalent to the applied along the disk diamet

).00003 to 0.3 MPa/s. For the low tensile stresses at the crack initiation point ranging from
t the salt cylindrical sample while temperature testing a cooling system is fabricated to tes
with temperature regulator are used loading. For the high temperature testing a heating tape
o 375 Kelvin. The time-dependent to apply constant temperature to the specimens from 348
d transient state component. The strain induced in salt consists of both instantaneous an

ıg. The cracks are induced at the inter-granular boundaries higher rather than cleavage slidi
ecreases results indicate that the tensile strength increases with increasing loading rate and d
sing the with increasing the temperature. The strengths decrease exponentially with decrea
ous the loading rates. The creep strain magnitude increase with temperature under var
from the loading rates. The tensile stress calculations are slightly higher than the tensile stress
simulation.

w can well describe the time-dependent behavior of salt. The law in derived by Exponential la
ep strain to stress and temperature. This equation can be used to predict the linking the cre
t tensile deformation of the salt under various constant temperatures. time-dependen

ilar the in-situ condition of mine roof and thus the The ring tension test on rock salt are sim
han those from the Brazilian tension test. It seems results from this study are more accurate
endent equations for deformability and strength are reasonable that the derive loading rate dep
le load such as mine roof, cavern roof and tunnel transferable to other salt rock under tensi

ations to long term salt roof. Limitations exist with regard to the application of these equ
ıder only transient creep storage cavern. Here, as a rule both deformability and strength are ur
or long term strength are phases and thus the proposed equations for steady-state creep phases
may normally not applicable.

Table 3. Parameters calibrated from ring tension test results.

Parameters	Values	R^2
ψ	-0.060	

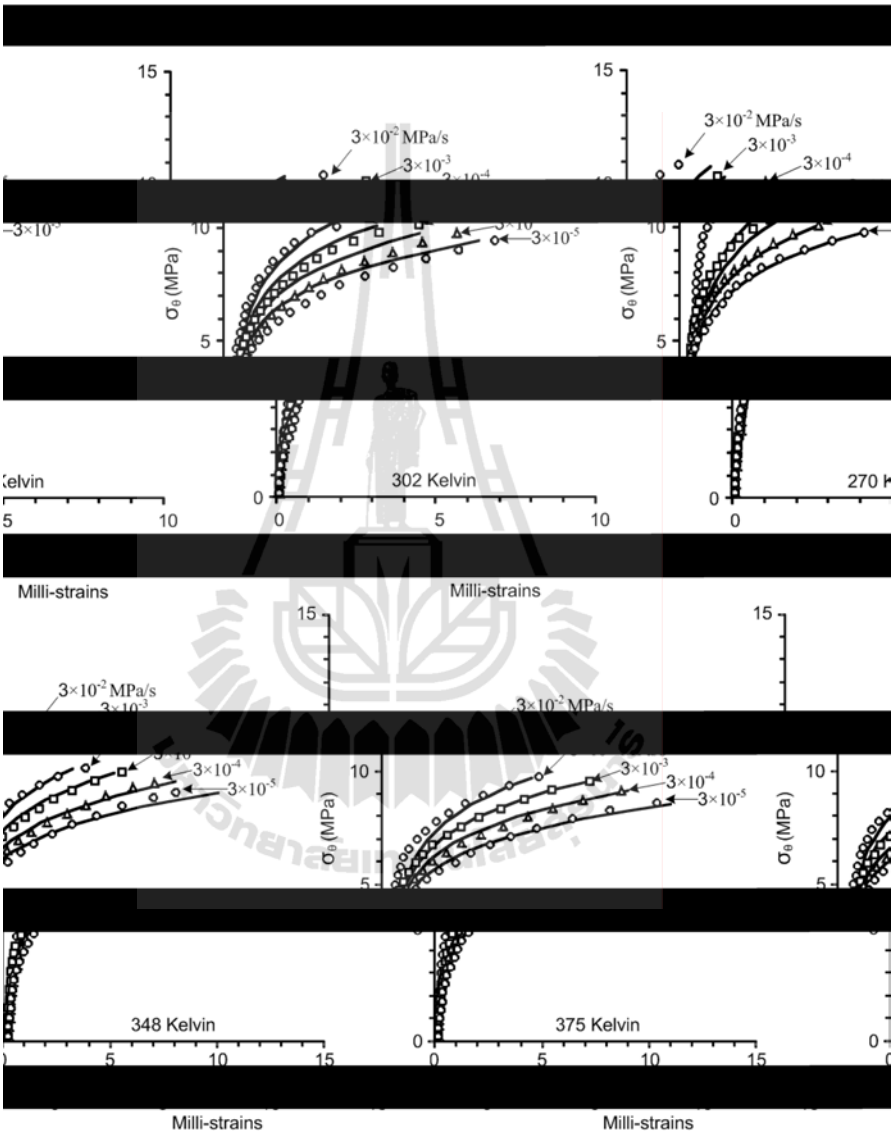

Figure 10. Comparisons between test results (points) and back predictions (lines).

CKNOWLEDGEMENTS **AC**

on This study was funded by Suranaree University of Technology and by the Higher Educati
er Promotion and National Research University of Thailand. Permission to published this pap
ng is gratefully acknowledged. We would like to thank Asean Potash Mining Co. for donati
salt cores used in this study.

REFERENCES

Continua, Version 4.0. Itasca. 1992. *User Manual for FLAC-Fast Langrangian Analysis of* Itasca Consulting Group Inc. Minneapolis, Minnesota.

ɔn Liang, W.G., Xu, S.G. & Zhao, Y.S. 2006. Experimental study of temperature effects c
ːk physical and mechanical characteristics of salt rock. *Rock Mechanics and Ro*
Engineering. 39(5): 469-482.

he Ripperger, E.A. & Davids, N. 1947. Critical Stresses in a Circular Ring. *Transactions of t*
ociety of Civil Engineering. 112(2308): 619-627. *American S*

983. *Review of Constitutive Laws used to Describe the Creep of Salt*. Senseny, P.E. 1
morial Institute, Columbus. Battelle Me

BIOGRAPHY

Mr. Sopon Wisetsaen was born on March 9, 1990 in Nakhon Ratchasima province, Thailand. He received his Bachelor's Degree in Engineering (Geotechnology) from Suranaree University of Technology in 2011. For his post-graduate, he continued to study with a Master's degree in the Geological Engineering Program, Institute of Engineering, Suranaree university of Technology. During graduation, 2011-2013, he was a part time worker in position of research assistant at the Geomechanics Research Unit, Institute of Engineering, Suranaree University of Technology.